January 2019

Determination Of Maximum Scour Depth For Spur Dikes Based On A Validated Two-Dimensional HEC-RAS Model

Mathew Lee Cox

DETERMINATION OF MAXIMUM SCOUR DEPTH FOR SPUR DIKES BASED ON A VALIDATED TWO-DIMENSIONAL HEC-RAS MODEL

Prepared by:

Mathew Lee Cox

Bachelor of Science, University of North Dakota, 2018

A Thesis

submitted to the Graduate Faculty

of the

University of North Dakota in

partial fulfillment of the requirements

for the degree of

Master of Science

Grand Forks, North Dakota

May 2019

This thesis, submitted by Mathew Lee Cox in partial fulfillment of the requirements for the Degree of Master of Science in Civil Engineering from the University of North Dakota, has been read by the Faculty Advisory Committee under whom the work has been done and is hereby approved.

4/25/2019

Dr. Yeo Howe Lim, Ph.D.
Associate Professor, Civil Engineering
Chairperson,

4/25/2019

Dr. Daba Gedafa, Ph.D.
Chair and Associate Professor, Civil Engineering

Dr. Gregory Vandeberg, Ph.D. 4/25/2019
Chair and Professor, Geography

This thesis is being submitted by the appointed advisory committee as having met all of the requirements of the School of Graduate Studies at the University of North Dakota and is hereby approved.

Dr. Chris Nelson
Dean, School of Graduate Studies

4/29/19
Date

PERMISSION

Title	DETERMINATION OF MAXIMUM SCOUR DEPTH FOR SPUR DIKES BASED ON A VALIDATED TWO-DIMENSIONAL HEC-RAS MODEL
Department	Civil Engineering
Degree	Master of Science

In presenting this thesis in partial fulfillment of the requirements for a graduate degree from the University of North Dakota, I agree that the library of this University shall make it freely available for inspection. I further agree that permission for extensive copying for scholarly purposes may be granted by the professor who supervised my thesis work or in his absence, by the Chairperson of the department or the dean of the School of Graduate Studies. It is understood that any copying or publication or other use of this thesis or part thereof for financial gain shall not be allowed without my written permission. It is also understood that due recognition shall be given to me and to the University of North Dakota in any scholarly use which may be made of any material in my thesis.

Mathew Cox

5/2/2019

Abstract

The introduction of spur dikes into a river flow field can have many far-reaching positive effects on the stability of a river channel. While the flow velocity directly at the spur dike tip or crest may increase, a large embayment area downstream of the spur dike will form with reduced flow velocities. Due to the increase in flow velocity at the spur dike, a scour hole will form. Scour is the leading cause of failure of hydraulic structures. In the past many hydraulic structures were tested by building scale prototype models, this method is very costly and hard to model all factors correctly. The recent introduction and widespread use of two-dimensional numerical models allow for increased efficiency and accuracy of hydraulic modeling. This recent breakthrough allows for relationships between dynamic variables and the estimated scour depth to be developed. The length of the spur dike and the flow rate were varied in the experiments. It was found that as the length of a spur dike increases, the depth of the scour also increases. This held a stronger correlation than the increase in flow rate. A relationship was developed between the maximum flow velocity, the upstream flow velocity, and the upstream Froude number to determine the maximum scour depth. This relationship proved to be more accurate than past relationships proposed using data from physical model analysis. The new relationship lowered the percent-error from 14% to 1% when the predicted scour depths were compared with the measured scour depths. The error was reduced from 7.3% to 1.6% for the long spur dike simulations and from 21.4% to 13.2% for the short spur dike simulations.

Table of Contents

List of Figures

List of Tables

Acknowledgments

I would like to thank Dr. Yeo Howe Lim for being my advisor over the past year. You have done an amazing job helping direct me in my studies and help me grow in my knowledge of water resources engineering. I would like to thank the North Dakota Water Resources Research Institute for helping fund this research and allowing me to spread my research throughout the region. I would like to thank Dr. Roger Kuhnle for his support from the United States Department of Agriculture with supplying the physical model data needed to complete the research. I would like to thank my parents for being supportive throughout the process and helping me with whatever came up. It meant the world to me. I would like to show great appreciation to my Thesis committee members, Dr. Daba Gedafa and Dr. Gregory Vandeberg from the Geography Department. They were a great help during my thesis work, as well as during my graduate course work. I have learned so much from them over the past year. I would like to thank the Civil Engineering Department and the College of Engineering and Mines as a whole for allowing me to conduct my research and further my career.

Chapter 1

1 Introduction

Harnessing the power of a river, while also being able to tame the river is important for sustainable development along the banks of a river. Lakes, oceans, and rivers are the main types of bodies of water. Rivers are the most dynamic of the three main types of water bodies when looking specifically at the movement component. Rivers continually flow and transport sediment. This causes rivers to meander and move vertically and laterally as they age. Even rivers that are on rocky surfaces can meander to great lengths, as shown by the Colorado River in the Grand Canyon. Rivers rarely flow in a linear direction and continually move. This causes problems when structures that are built close to a river do not move as the channel moves.

Open channel flow is an essential topic in hydraulics and studies of this topic range from drainage in artificial channels and rivers (Ying et al., 2004; Burguete et al., 2008), the design of hydraulic structures such as spillways (Unami et al., 1999) and bridges (Biglari and Sturm, 1998) to flood prevention measures (Hsu et al., 2003). Rivers have been used as a source of water, for obtaining food, for transportation use, as a defensive measure, and as a source of hydropower for thousands of years (Krishna et al., 2015). Historically, civilizations have developed close to large bodies of water, such as lakes, rivers, and oceans due to the necessity for food and water. Some of these civilizations learned to thrive near rivers that would flood regularly as in the Nile River in northeast Africa.

1.1 Problem Statement

As time passes, rivers in low-lying areas continue to move and create new flow paths through the meandering process. Homes and structures that may have been built in a safe place far from a river bend 50 years ago, may now be in danger of riverbank sluffing and total loss of the structure. Outer banks of river bends are usually associated with scour and erosion (Fazli, 2008). Where the bank material is erodible, streams and rivers often erode the banks and move laterally, resulting in land loss, channel change, excessive sediment yield and degradation of the water quality (Kuhnle & Alonso, 2013). This is where the importance of riverbank stabilization is key.

The design of riverbank stabilization techniques has been hampered by incomplete research and minimal design guidelines for specific river instances. Riverbank stabilization also helps reduce sediment transport in a river. A reduction in water velocity at the outside bend of a river reduces the amount of erosion and sediment that a river can transport. Predicting the cause of riverbank erosion and preventing further erosion is the main aim of riverbank protection. Vegetation can act as a protection to the riverbanks. Sometimes this vegetation cover has been destroyed by human activities resulting in bank erosion (Prasad et al., 2015). Rivers develop different flow patterns, such as braided and meandering, depending on the discharge regime, sediment load, hydrodynamic forces and floodplain properties (Allen, 1985; Garde, 2012). Impacts of riverbank erosion are multifarious: social, economic, health, education, and sometimes political (Prasad et al., 2015).

1.2 Study Focus

Spur dikes have been used extensively in all parts of the world as river training structure to enhance navigation, improve flood control, and protect erodible banks. The

effect of the spur dike is to reduce the flow velocity along the streambank, thereby reducing the erosive capability of the stream and, in some cases, inducing sedimentation between dikes (Copeland, 1983). Spur dikes are one of the most widely used structures in hydraulic engineering (Cao et al., 2013). Spur dike may be defined as a structure extending outward from the bank of a stream for the purpose of deflecting the current away from the bank to protect it from erosion (Kuhnle & Alonso, 2013). The water surface rises before the spur dike and it lowers beside the nose and behind the spur dike (Giglou et al, 2017). Despite the widespread use of spur dikes, many aspects of their design are based on prior experience and are only applicable to streams and rivers of a similar nature (Copeland, 1983). Parameters affecting spur dike design include width, depth, velocity, and sinuosity of the channel; size and transportation rate of the bed material; cohesiveness of the bank material; and length, width, crest profile, orientation angle, and spacing of the spur dike (Copeland, 1983).

1.3 Hypothesis

Determination of procedure to estimate the maximum scour depth and volume of scour by using two-dimensional (2D) numerical modeling software. The software does not have the ability to perform 2D sediment transport and thus a relationship between maximum scour depth and a 2D numerical model will need to be developed.

1.4 Research Goals

Development of hydraulic modeling software has progressed greatly in recent years. HEC-RAS developed its first version of hydraulic modeling software in 1995 with HEC-RAS 1.0 (Brunner, 2016). The software has steadily increased in power and adaptability. The original version only solved hydraulic problems in one-dimension (1D).

This causes problems when attempting to model complex structures that may have eddy formations and inconsistent water velocities across the width of the channel. With the release of HEC-RAS 5.0, two-dimensional (2D) modeling was introduced (Brunner, 2016). This added capability allows for a full velocity field to be determined as well as the locations of eddy formations. This feature had been available on other modeling software in the past but the other software needed a license subscription and thus the availability of the software was extremely limited. HEC-RAS software has always been open to the public and free-of-charge. With the introduction of 2D modeling capabilities, complex hydraulic structures such as bend way weirs, spur dikes, wing walls, and more are able to be modeled accurately. Accurate and efficient modeling allows for the design process to determine the most suitable design for the structure.

The objective of this research is to develop plan-view design guidelines for spur dike design that can be used with the software HEC-RAS. HEC-RAS will be used to perform a two-dimensional flow analysis on a proposed three-dimensional (3D) surface that contains a spur dike field in the river channel. The analysis will use geometric and flow data from the United States Bureau of Reclamation physical model that was developed to test spur dikes in a scaled-down form. The physical model results will then be used to verify the results determined from the HEC-RAS two-dimensional model. This will allow for the determination of the validity of continued use of the HEC-RAS software for spur dike design. The research will bring together individual research performed by other researchers while implementing the new modeling capabilities of HEC-RAS.

Chapter 2

2 Literature Review

2.1 HEC-RAS

The Hydrologic Engineering Center first designed the River Analysis System (HEC-RAS) in 1997 and has been continually developed to version 5.0.7 currently (US Army Corp of Engineers, 2019). HEC-RAS version 5.0.5 will be used in this research, as 5.0.7 was recently made available and there may still be bugs within the newer version of the software program. HEC-RAS has the ability to solve hydraulic problems using one-dimensional steady flow, one and two-dimensional unsteady flow, sediment transport, and water quality modeling. The Saint-Venant or Diffusion Wave equations are used to model the flow in the open channel in two dimensions.

The Saint-Venant equation is derived from the Navier-Stokes equation when solved for shallow water flow conditions. The Navier-Stokes equation was developed by Claude-Louis Navier and George Gabriel Stokes (Sturm, 2009). The equation describes the motion of viscous fluid substances by applying Newton's Second Law of Motion to fluid flow. The Navier-Stokes equations can be used to model weather, pipe flow, expanding and contracting flow, flow around an airplane wing, and ocean current flow. The Navier-Stokes equation for two dimensions is shown in Equations 1 and 2, where u is velocity, t is time,

ρ is density, V is viscous forces, f is gravitational forces, and x and y subscripts denote the direction.

$$\frac{\partial u_x}{\partial t} + u_x \frac{\partial u_x}{\partial x} + u_y \frac{\partial u_x}{\partial y} = -\frac{1}{\rho}\frac{\partial p}{\partial x} + V\left[\frac{\partial^2 u_x}{\partial x^2} + \frac{\partial^2 u_x}{\partial y^2}\right] + f_x \qquad (1)$$

$$\frac{\partial u_y}{\partial t} + u_x \frac{\partial u_y}{\partial x} + u_y \frac{\partial u_y}{\partial y} = -\frac{1}{\rho}\frac{\partial p}{\partial y} + V\left[\frac{\partial^2 u_y}{\partial x^2} + \frac{\partial^2 u_y}{\partial y^2}\right] + f_y \qquad (2)$$

Within the HEC-RAS software, a Full Momentum or Diffusion Wave solver can be used to determine the flow field of a given situation. The Saint-Venant equation was developed by Adhémar Jean Claude Barré de Saint-Venant (Sturm, 2009). The Saint-Venant equation is a shallow water equation, meaning that the horizontal scale is much greater than the vertical scale. This derivation is done by depth-integrating the Navier-Stokes Equation. Depth-integration allows for the vertical velocity to be removed from the equation. This does not mean that the vertical velocity is 0 but that it is assumed to be negligible when compared with the horizontal velocity components. The Saint Venant equation is derived from the Navier-Stokes equation and is shown in Equations 3, 4, and 5. Equation 3 is the continuity equation, Equation 4 is the momentum equation in the *x*-direction, and Equation 5 is the momentum equation in the *y*-direction, where *h* is the depth of flow, *u* is the velocity in the *x*-direction, *v* is the velocity in the *y*-direction, z_b is the height deviation of the pressure surface, and *n* is the roughness coefficient (Manning's n).

$$\frac{\partial h}{\partial t} + \frac{\partial (hu)}{\partial x} + \frac{\partial (hv)}{\partial y} = 0 \qquad (3)$$

$$\frac{\partial(hu)}{\partial t}+\frac{\partial(hu^2)}{\partial x}+\frac{\partial(huv)}{\partial y}+gh\frac{\partial h}{\partial x}=-gh\frac{\partial z_b}{\partial x}-gn^2u\frac{\sqrt{u^2+v^2}}{h^{1/3}} \quad (4)$$

$$\frac{\partial(hv)}{\partial t}+\frac{\partial(hv^2)}{\partial x}+\frac{\partial(huv)}{\partial y}+gh\frac{\partial h}{\partial y}=-gh\frac{\partial z_b}{\partial y}-gn^2v\frac{\sqrt{u^2+v^2}}{h^{1/3}} \quad (5)$$

The Saint-Venant equation is further reduced to the Full Momentum equation to solve the water surface elevation within HEC-RAS. The Full Momentum equation is shown in Equation 6 and 7 The Full Momentum equation is used within HEC-RAS to solve for the water surface profile, as well as velocity and flow direction.

$$\frac{\partial v}{\partial t}+u\frac{\partial v}{\partial x}+v\frac{\partial v}{\partial y}=-g\frac{\partial H}{\partial y}+v_t\left(\frac{\partial^2 v}{dx^2}+\frac{\partial^2 v}{\partial y^2}\right)-c_f v+fu \quad (6)$$

$$\frac{\partial u}{\partial t}+u\frac{\partial u}{\partial x}+v\frac{\partial u}{\partial y}=-g\frac{\partial H}{\partial x}+v_t\left(\frac{\partial^2 u}{dx^2}+\frac{\partial^2 u}{\partial y^2}\right)-c_f u+fv \quad (7)$$

The Diffusion Wave equation in two dimensions is shown in Equations 8, 9, and 10. The Diffusion Wave equation assumes that inertial forces are less than gravity, friction, and pressure forces. This is done by disregarding unsteady, advection, turbulence, and Coriolis terms that may be included in the Full Momentum equation. In general, the 2D Diffusion Wave equation allows the software to run faster and has greater stability properties, while the 2D Saint-Venant (Full Momentum) equations are applicable to a wider range of problems (Brunner, 2016).

$$-\nabla H=\frac{n^2|V|V}{(R(H))^{4/3}} \quad (8)$$

The Diffusion Wave General equation is the default setting to allow for quicker processing within HEC-RAS. The software allows for ease of switching between the two equations, either can be used to solve a hydraulic problem. HEC-RAS recommends running the software in both Diffusion Wave and Full Momentum to determine if there is a large difference in the water surface elevation or flow velocity. For the Full Momentum equation

to be used, the computational time step may need to be reduced to allow for a stable simulation as discussed later in the Courant Number section.

Equation 9 shows the Diffusion Wave Approximation of Shallow Water Equations with Equation 10 showing the calculations for variable β in Equation 9. The system of equations originally given in the Full Momentum equations can be reduced to this one equation. This allows for expedited analysis and reduced processing time, with the reduction in parameters and equations to be solved. The difference in modeling a spur dike field with the Diffusion Wave and Full Momentum equations is shown in Figure 1.

$$\frac{\partial H}{\partial t} - \nabla \cdot \beta \nabla H + q = 0 \tag{9}$$

$$\beta = \frac{(R(H))^{5/3}}{n|\nabla H|^{1/2}} \tag{10}$$

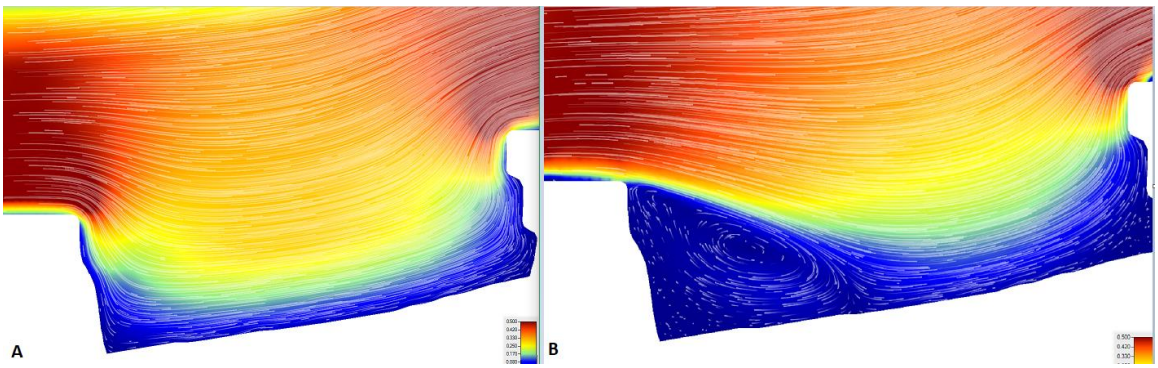

Figure 1: Diffusion Wave (A) vs. Full Momentum (B)

There is a noticeable difference between the two equation methods in the mapping output. The flow field in the Diffusion Wave method expands and contracts evenly before and after the spur dike with no eddies forming. Whereas in the Full Momentum mapping output on the right, there is multiple eddy formation occurring and the flow field flows as expected. This comparison demonstrates the differences between the two methods.

The Diffusion Wave method is suitable for terrain with minimal contraction and expansion areas but lacks the precision of the Full Momentum method, when there are drastic changes in the flow area, such as in the vicinity of a spur dike or other hydraulic structure. It is important to perform this sensitivity analysis when developing a hydraulic model. The water surface elevation and location of eddies can change greatly when using the Diffusion Wave or Full Momentum methods. The Full Momentum method is more accurate but takes longer to run and can crash due to instability issues more easily than the Diffusion Wave.

To solve the 2D unsteady flow equations, an Implicit Finite Volume algorithm is used. This allows the 2D flow areas to cycle from wet to dry, as well as handle subcritical, supercritical, and mixed flow regimes (Brunner, 2016), which promotes improved stability and robustness when compared with traditional finite difference and finite element techniques. The Implicit Finite Volume Method (IFVM) represents partial differential equations in the form of algebraic equations (LeVeque, 2002).

HEC-RAS uses a “high-resolution sub-grid model” to analyze a three-dimensional terrain mesh. The cells in HEC-RAS can have up to 8 sides. Each cell has a detailed volume/area relationship that represents the underlying terrain (Brunner, 2016). HEC-RAS uses cross-sections of the grid as the cell faces. This allows for detailed flow data to be computed from larger cell sizes than previously available with other techniques. A sample of the high-resolution sub-grid model is shown in Figure 2.

Many 2D models use a computational cell that has a flat bottom and treats each cell face as a straight line with a single elevation. HEC-RAS 2D calculates detailed hydraulic table properties for each cell and cell face (Lintott, 2017). This is done at the beginning of

each analysis run. Each cell shown in Figure 2 will have the properties calculated at the center, shown as the black dot. A cell is denoted by a single black grid space with a black dot to signify the geometric center of the cell.

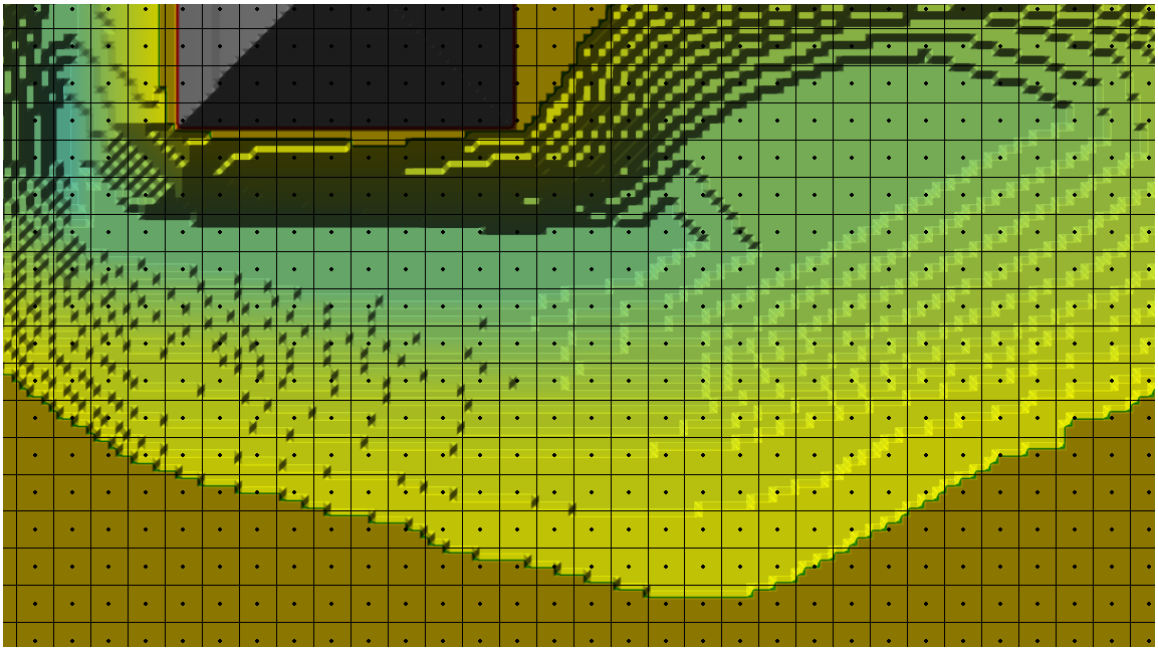

Figure 2: High-Resolution Sub-Grid [Color variations show the height of that location. Brown: initial bed level, Light Blue: deepest parts of the scour, Gray: spur dike]

HEC-RAS uses an extension called RAS Mapper to increase the functionality without the need for outside software (Brunner, 2016). RAS Mapper allows for the integration of GIS-style tools into HEC-RAS. Three-dimensional surfaces can be imported and edited within RAS Mapper. This is an important tool for surface manipulation, if the imported surface is LiDAR-based then it may have unwanted structures in the raster format. These structures could be bridges, culverts, dikes, trees, houses, roads, or other structures that may inhibit the correct hydraulic analysis of the area. These structures affect the flow and roughness of a channel and may be accounted for in varying ways. RAS

Mapper also allows for viewing of 2D flow fields after analysis by depth, water surface elevation, and velocity (Brunner, 2016). These values can be shown as a maximum value during the analysis or as a time-series video of the changes in the parameter during analysis.

The Courant number is used to determine if a mesh and computational time step are compatible (Brunner, 2016). The Courant number is a relationship between the wave celerity (ft/s), computational time step (s), and average cell size. The Courant number has a suggested maximum of 3 for the Saint-Venant equation and 5 for the Diffusion Wave equation (Brunner, 2016). The formula for determining the Courant Number is shown in Equation 11. The Courant number is ideally set to a value of 1 to determine the computational time step. This is unachievable in some circumstances and must be set at a higher value to allow for reasonable run times based on the number of cells in the two-dimensional flow area.

$$C = \frac{V\,\Delta T}{\Delta X} \tag{11}$$

The Transverse Mixing Coefficient (D_t) can be used in determining the flow path and flow directions around spur dikes and other hydraulic structures. HEC-RAS allows the user to set the coefficient to a value between 0 and 5. The default value is 0 and must be changed for problems involving high levels of contraction and expansion. The range of values is shown in Table 1. When the Eddy Viscosity Mixing Coefficient is used, the time step must be reduced to allow for the software to run stably.

The Eddy Viscosity Mixing (EVM) coefficient (v_t) is calculated using Equations 12 and 13. The EVM is only used with the Full Momentum equations. It is important to note that the inclusion of the Eddy Viscosity Mixing Coefficient value above 0 increases

the length of the Full Momentum equation with substantial increases in computational analysis time and instability within the model.

Table 1: Eddy Viscosity Mixing Coefficient (Brunner, 2016)

D_T	**Mixing Intensity**	**Geometry and Surface**
0.11 – 0.26	Small Transversal Mixing	Straight Channel Smooth Surface
0.3 – 0.77	Moderate Transversal Mixing	Gentle Meanders Moderate Irregularities
2.0 – 5.0	Strong Transversal Mixing	Forceful Meanders Rough Surface Strong Irregularities

$$v_t = D_t h u_* \quad (12)$$

$$u_* = \sqrt{gRS} = \frac{\sqrt{g}}{C}|V| = \frac{n\sqrt{g}}{R^{1/6}}|V| \quad (13)$$

2.2 Scour and Scour Holes

Local scour is caused by the erosive forces from flow turbulence acting on the erodible bed in the vicinity of an obstacle or structure placed in a stream, such as a spur dike or a bridge pier (Duan et. al., 2009). Bed shear stress near the dike can be 6 to 8 times as large as that of the approaching flow so that a local scour is developed near the dike without the shear stress of approaching flow exceeding the critical shear stress of bed material (Duan et al., 2009).

An important consideration in designing a spur dike is to predict the depth of bed scour produced by flow (Fazli, 2008). The key drivers behind the scour depth are the water velocity and the bed material, as shown in Equation 14. As bed material becomes finer and less dense, the ability for sediment transport and development of scour holes greatly increases. Mean bed-shear stress or near-bed velocity were traditionally used for estimating the rate of sediment transport (Duan et al., 2009).

$$\tau_0 = \gamma R S_w \tag{14}$$

Bridge abutments affect flow in many ways similar to spur dikes (Kuhnle & Alonso, 2013). Both bridge abutments and spur dikes constrict the flow path and thus increase the flow velocity in the restricted area. Constructing spur dikes causes contraction of the flow path and as a result, increasing flow velocity (Giglou et al., 2017). It is interesting to note that none of the present methods are able to accurately predict the scour dimensions around the spur dike in a curved channel (Fazli et al., 2008), thus a physical model must be constructed to accurately model the curved channel scour.

The presence of any protection measure at the outer bank generally modifies the bend flow pattern and hence causes bed deformation (Przedwojski, 1995). In laboratory experiments done on a flume by Bhuiyan (2010) and Kuhnle et al (1999), it is shown that immediately after the installation of a hydraulic structure, bed scour and deposition occur rapidly. Eventually, a dynamic equilibrium condition is reached when local scour effectively ceases, showing that scour diminishes over time with constant flow. During Kuhnle's (1999) flume experiments, dynamic equilibrium was achieved between 30 and 133 hours after flow began in the channel. If flow increases (e.g. flooding conditions) then the scour could begin again with the increase in flow rate and continue after the flood

recedes until dynamic equilibrium is achieved again. If conventional spurs are constructed on a river bend, the bank between the adjacent structures often continues to retreat up to a certain limit forming an embayment in the bank (Bhuiyan et al., 2010).

The spacing of the spur dikes plays a key role in the size and depth of the scour holes. When the space between two spur dikes is less than 2.6 times the spur dike length, the relative maximum scour depth for the two spur dikes will be smaller for all situations of spur dikes in a bend (Fazli et al., 2007). When the spacing is greater than 2.6 times the spur dike length, the relative maximum scour depth for the two spur dikes will increase with increasing ratios of relative space between them (Falzi et al., 2007). Thus as the space between the spur dikes increase, the flow begins to return to normal and then must be restricted again causing increased erosion.

The width of the spur dike must be designed with many factors in mind, as well as done economically, to reduce excessive erosion. The length of the vortex zone near the water level is longer than at depth in the channel. The vortex zone extends approximately four times the spur dike length downstream of the spur dike from the downstream of the spur dike, for a width of 1.2 times the spur dike length (Giglou, 2017). This means that the vortex zone is longer at the surface of the water than at the channel bottom.

Melville (1992) developed a technique for predicting the maximum scour depth, which was then used to predict the volume of scour by Kuhnle (1999). Melville (1992) developed the relationship specifically between bridge abutments and scour, but in many situations, local scour at bridge abutments and spur dikes are very similar. The main difference between Melville (1992) and Kuhnle (1999) is that the Melville relations were

found with flows below the top of the spur dike, whereas Kuhnle used flows that overtopped the spur dike.

The maximum scour depths developed by the physical model in the Kuhnle (1999) study consistently overpredicted the scour depths. The mean value of the ratio of measured to calculated scour depths for the data of this study was 0.56 (Kuhnle et al, 1999). Kuhnle (1999) adopted a modified Melville equation for predicting scour, the leading coefficient is multiplied by 0.56 to bring the prediction in line with the measured results. The original and modified Melville equations are shown in Equation 15 and 16, respectively.

$$\frac{d_s}{Y_\infty} = 2K_M\eta^{(1-\delta)} \tag{15}$$

$$\frac{d_s}{Y_\infty} = 1.12K_M\eta^{(1-\delta)} \tag{16}$$

The K_M parameter represents the effect of flow intensity, flow depth, sediment size, sediment gradation, abutment length, abutment shape and alignment, and approach channel geometry. Upon review of the experimental data, Kuhnle (1999) decided to use the shear velocity ratio for K_M. This was used in place of the mean velocity ratio U/U_c used by Melville (1992) due to the difficulty of accurately calculating the critical mean velocity in many of the flows (Kuhnle et al, 1999).

A relationship between the volume of the scour hole and the depth of the scour was obtained and used to predict the volume of the scour hole by Kuhnle (1999). Equation 17 shows the relationship between the maximum scour depth and the total volume of scour. The total volume equation only uses the length and approach depth parameters to determine the volume of scour. This is done because the K_M value (representing flow conditions) is

already included in the equation for determining maximum scour depth. The larger overtopping ratios (Y/H) caused the region of maximum scour to shift toward the channel bank and caused secondary scour zone to form downstream of the spur dike (Kuhnle et al, 1999), but this is not represented in the equation in any form.

$$\frac{V_{30}}{(d_{s30})^3} = 17.106\left(\frac{L}{Y_\infty}\right)^{-0.781} \quad (17)$$

Kuhnle (1999) demonstrated that when spur dikes are spaced such that each structure is independent of adjacent structures, then increasing spur length from 2.5 to 5 m would lead to an approximate doubling of pool volume, with the possibility for a much greater increase in pool volume. Here pool volume is detailed as the total volume of the scour holes formed by a spur dike.

Kuhnle (1999) developed scour hole dimension relationships based on the flow and length of the spur dikes. The data is shown in Table 2 with a reference sketch shown in Figure 3. This comparison shows that the channel width is the limiting factor in determining the overall width of the scour hole in the long spur dike trails. This is shown

Table 2: Scour Hole Dimensions as Ratio of Spur Dike Dimensions (Kuhnle et al, 1999)

Run ID	a/L	b/L	c/L	d/L
L90-1	4.0	0.8	1.9	6.0
L90-2	4.0	0.7	1.7	4.9
L90-3	3.4	0.0	1.6	7.7
L90-4	4.0	0.0	1.6	10.2
S90-1b	5.4	0.5	2.5	7.6
S90-2b	4.0	1.0	1.0	4.7
S90-3	4.5	0.7	1.6	5.8
S90-4	5.4	0.0	2.2	9.4

by the scour hole reaching all the way across the channel bottom. This shows the need for a larger flume width to determine the true extents of the scour hole.

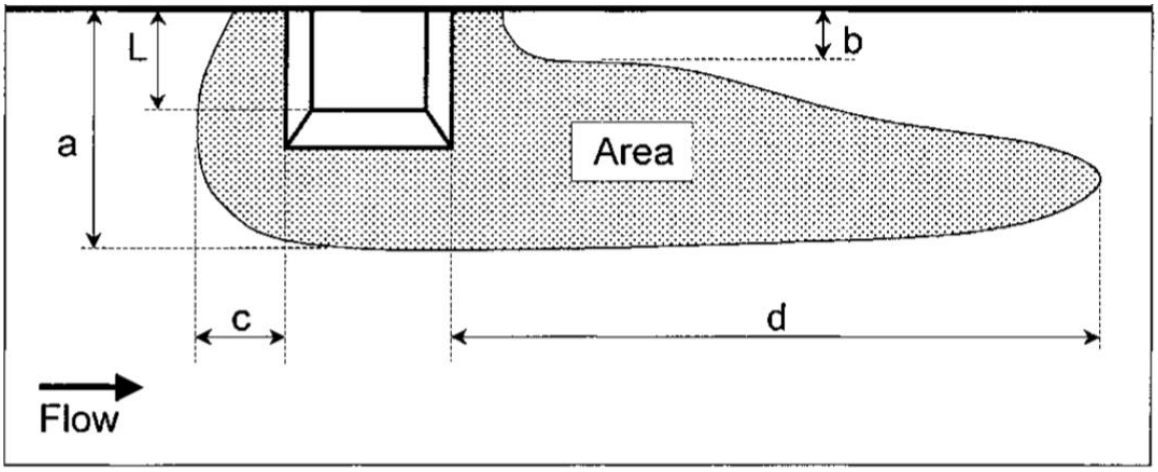

Figure 3: Definition Sketch for Ratios in Table 2 (Kuhnle et al, 1999)

2.3 Types of Spur Dikes

Spur dikes, as shown in Figure 3, can be built out of three main materials. These include wood, rip-rap, and concrete. Wood spur dikes are normally found along beaches and consist of wooden piles that are driven into the sand. The purpose of a wooden pile spur dike is to reduce horizontal migration of sand down a beach.

Concrete spur dikes are commonly the smallest of the spur dikes and only extend a short distance into the flow field. Concrete spur dikes are costly to build and can fail easily if large scour holes develop. Concrete spur dikes are also called hard-points. Hard-points add roughness and localized bank stability (Biedenharn and Watson, 1997) to stabilize a riverbank section.

Another type of spur dike is built with sheet-pile. Sheet-pile is driven into the channel bed and bank to create a vertical wall in the flow field. Sheet-pile spur dikes are rarely used due to the need for large equipment in the river channel. Rip-rap spur dikes are

the most commonly built version and are used for many applications. Rip-rap spur dikes are denoted as semi-permeable due to the gaps in between the rock that allows a small portion of water to pass at a reduced flow rate. Rip-rap spur dikes can also be fitted with "launch-rock." Launch-rock is used to fill scour holes that may develop from the implementation of the spur dike. The rock is "launched" into the scour hole to fill and stabilize the hole.

2.4 Spacing

The spacing of spur dikes is extremely important. Spur dikes that are spaced too close together become expensive and are over-engineered, whereas spur dikes spaced too far apart may not protect the bank as designed. Spur dikes will interact with each other in a certain range, beyond which they are independent (Cao et. al, 2013, Ying & Jiao, 2004). The spacing between spur dikes has generally been related to effective length (Copeland, 1983). Effective length is designated as the distance that the spur dike extends into the channel normal to the bank. A spur dike that is oriented upstream or downstream would need to have a longer total length to have the same effective length that a perpendicular spur dike would have, as shown in Figure 4. Figure 4 also shows incoming flow depth, the top width of the spur dike, and height. These are all important parameters when designing spur dikes.

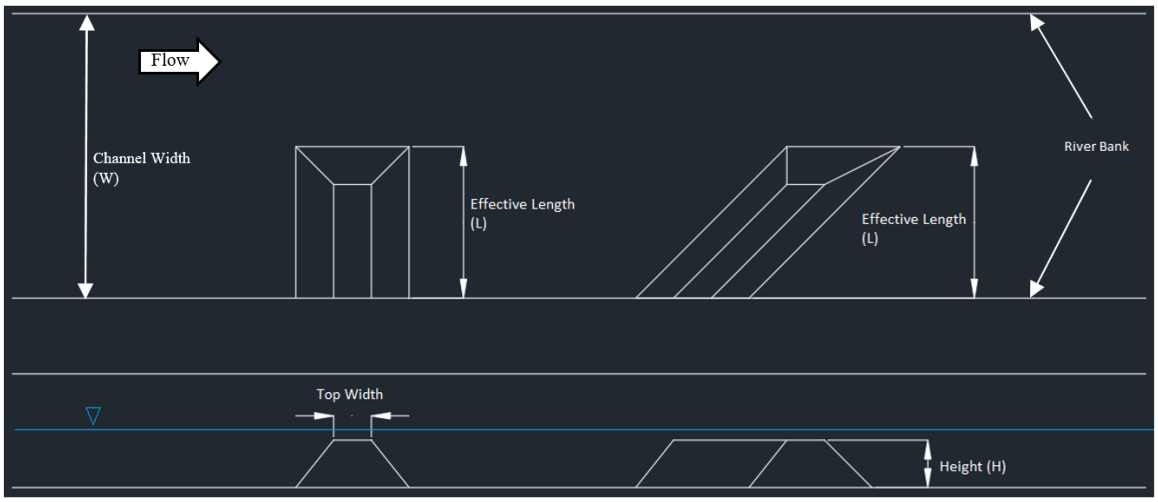

Figure 4: Effective Length vs. Length of Spur Dikes (Top: Plan View, Bottom: Profile View)

Spur dike groups can be classified as large-scale and small-scale groups according to their interaction with each other. The most common use of spur dikes is in shallow, wide streams with moderate to high suspended sediment loads (Baird et al., 2015). There is no agreed upon definition between large- and small-scale groupings.

2.5 Orientation

Spur dikes are generally constructed with a downstream angle or perpendicular to the bank line tangent for bank protection purposes (Lagasse et al., 2009). Spur dikes oriented in the upstream direction generally protect less bank length downstream of the spur tip for the same spur length, have greater scour depth at the tip, and increase hydraulic roughness (Baird et al., 2015). Spur dikes oriented 90° results in the greatest benefit for their length and are recommended to reduce tip scour (Baird et al., 2015). Orienting a spur dike at 90° maximizes the effective length and thus is the most cost-efficient building method.

2.6 Sedimentation

Sedimentation around spur dikes and other hydraulic structures is one of the most important issues (Giglou et al., 2017) in the design of hydraulic structures. The amount of sedimentation at the first spur dike location is greater than that at the second spur dike and likewise at the second is greater than that at the third and at the is more than the at the fourth one (Mohammad et al., 2016). Sediment particles can be transported by the flow of water in the form of bed-load and suspended load, depending on the size of bed material particles and flow conditions. (Mohammad et al., 2016). Particles only remain in suspension when the turbulent eddies have dominant vertical velocity components exceeding the particle fall velocity (Mohammad et al., 2016). Thus, when a spur dike, or other obstruction, is introduced to the flow field reduces in the obstructed area allowing particles to fall out of the water downstream of the obstructed areas.

Chapter 3

3 Methodology

3.1 Dimensional Analysis

The scour geometry around a spur dike depends on channel geometry, spur dike characteristics, flow conditions, and sediment properties (Fazli et al, 2008). These parameters are defined as channel width for channel geometry, length and height of spur dike for spur dike characteristics, upstream flow depth, upstream flow velocity, and maximum velocity for flow conditions, and median grain size for sediment properties.

$$d_s = f\left(W, L, H, Y_\infty, V_{max,}\, V_1, d_{50}\right) \tag{18}$$

These parameters can be reduced using dimensional analysis to:

$$\frac{d_s}{Y_\infty} = f\left({W}/{H}, {L}/{Y_\infty}, {H}/{W}, {Y_\infty}/{H}, {V_{max,}}/{V_1}, {d_{50}}/{W}, Fr\right) \tag{19}$$

The Froude number (Fr) is the ratio of flow velocity to the square root of gravity and hydraulic depth, shown in equation 20.

$$Fr = \frac{V}{\sqrt{gD}} \tag{20}$$

These parameters are further reduced by simplification of removing constants:

$$\frac{d_s}{Y_\infty} = f\left({L}/{Y_\infty}, {Y_\infty}/{H}, {V_{max,}}/{V_1}, Fr\right) \tag{21}$$

The concept of maximum velocity ratio within a structure field as compared to baseline conditions was quantified and predictive methodologies were originally developed by Heintz (2002). A dimensional analysis was done by Scurlock (2012) and Fazli (2008) on plan view parameters for spur dike analysis. These parameters are ones that could be seen from the air. These dimensional analyses produced variables that are very similar to the ones determined within this dimensional analysis.

3.2 Parameters

Variable Parameters

The input parameters are listed below. These parameters were varied to produce the analysis outputs from HEC-RAS. The Manning's n, computational grid spacing, and computational time step were all kept constant to allow for ease of analysis and comparison. The length of the spur dike was either 0.305 m for the long spur dike setup or 0.152 m for the short spur dike setup. The parameters are shown in Table 3.

Table 3: Input Parameters (HEC-RAS)

Run ID	Flow (m^3/s)	Length (m)	Manning's n	Computational Grid Spacing (m)	Computational Time Step (s)	Bed Condition
L90-1	0.072	0.305	0.037	0.05	0.1	Scoured
L90-2	0.072	0.305	0.037	0.05	0.1	Scoured
L90-3	0.144	0.305	0.037	0.05	0.1	Scoured
L90-4	0.144	0.305	0.037	0.05	0.1	Scoured
S90-1b	0.072	0.152	0.037	0.05	0.1	Scoured
S90-2b	0.072	0.152	0.037	0.05	0.1	Scoured
S90-3	0.144	0.152	0.037	0.05	0.1	Scoured
S90-4	0.144	0.152	0.037	0.05	0.1	Scoured
L90-10	0.072	0.305	0.037	0.05	0.1	Flat
L90-11	0.144	0.305	0.037	0.05	0.1	Flat
S90-10	0.072	0.152	0.037	0.05	0.1	Flat
S90-11	0.144	0.152	0.037	0.05	0.1	Flat

The Run ID will remain constant throughout the analysis and comparison to allow for ease of reading.

3.3 AutoCAD Civil 3D

The three-dimensional (3D) surfaces used in the analysis of the flow area were developed using AutoCAD Civil 3D (Civil3D) (AUTODESK, 2019). This program allows for robust surface building to occur. The validation model was constructed within Civil3D using a point group system. This system allows for the dynamic, systematic building of the surface through a collection of points. These points can be spaced close or far apart to achieve the desired 3D surface. The points are assigned a location, elevation, and group value. The group value allows for points to be labeled as what they are showing, such as a culvert invert elevation could be shown as C_INV. Figure 5 shows the informational set up of the points in Civil3D. The desired precision of the points can be set depending on the need of the user. The points default to show two decimal places for ease of viewing during creation and manipulation of the surface.

Figure 5: Point Description (AutoCAD Civil3D)

A bounding region is then created to limit the extents of the surface. Without a bounding region, the surface may extrapolate outwards and cause errors in the surface

during analysis. The surface can be exported as a GeoTIFF with user-defined precision. This allows for ease of import into the HEC-RAS software via the RAS Mapper extension. When exporting a surface to use in hydraulic analysis, the resolution is a key factor in how the analysis runs. Resolutions of 0.100, 0.010, and 0.001 meters are shown in Figure 6.

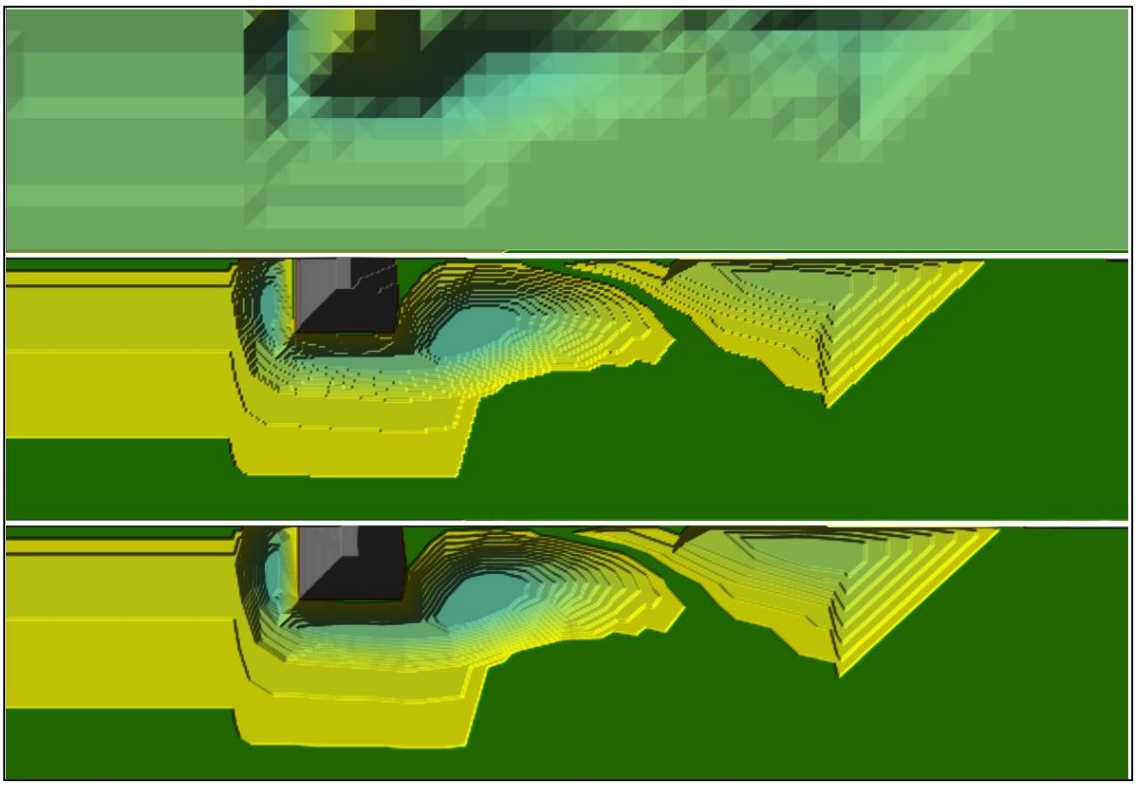

Figure 6: AutoCAD Surface Resolution Output [Top (A): 0.1m, Middle (B): 0.01m, Bottom(C): 0.001m]

There is a noticeable difference between Surface A and B with a smaller difference between B and C. The analysis outputs changed drastically from the coarsest to the finest surface inputs. The analysis outputs are shown in Figure 7. These show the large differences between the coarse and fine surfaces. A resolution of 0.01m for the exporting of surfaces from Civil3D to HEC-RAS will be used throughout the remainder of the

analysis. This will allow for quicker exporting of surfaces, as well as minimizing computation times.

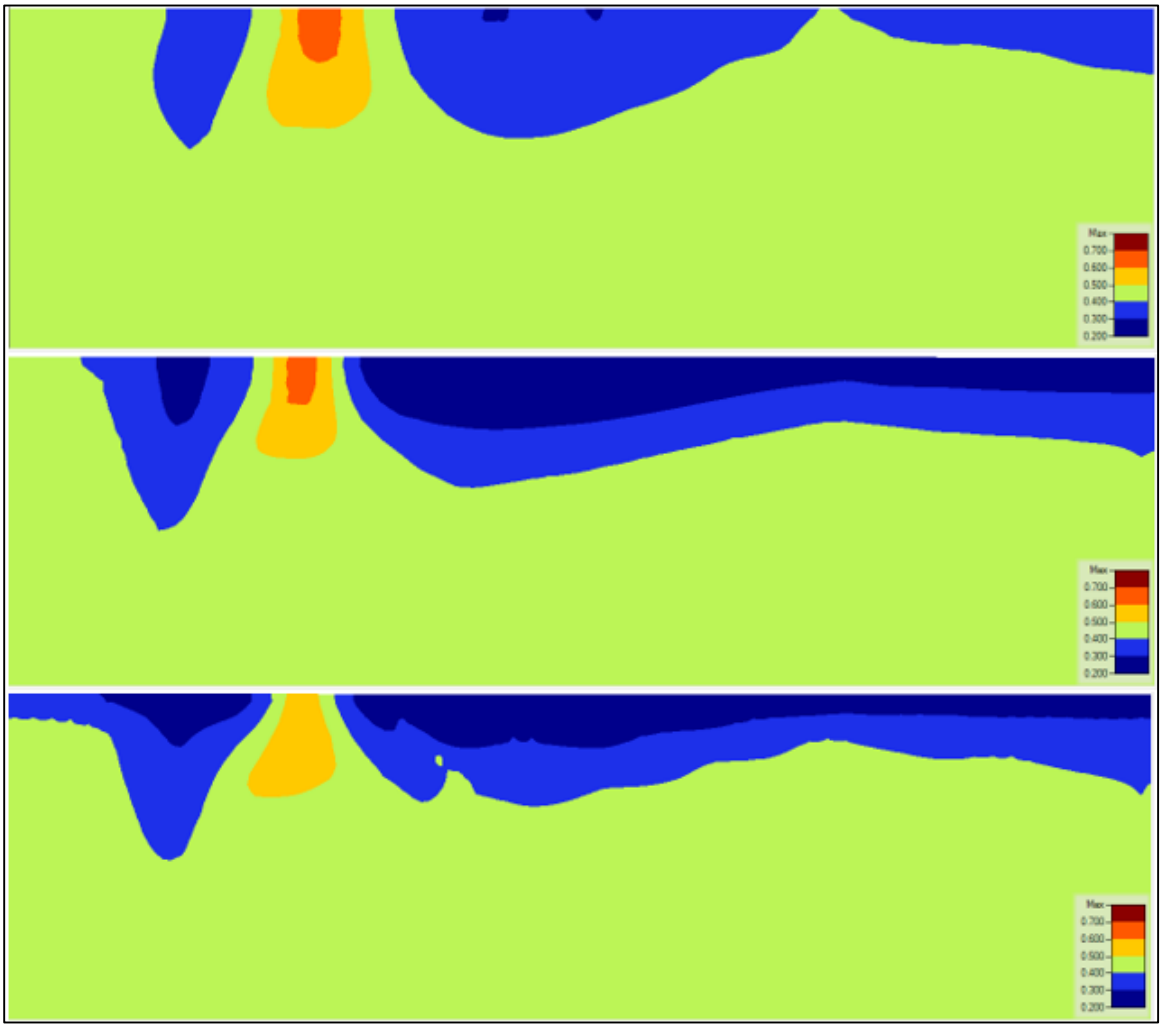

Figure 7: Civil 3D Mesh Fineness Comparison [Top: 0.1m, Middle: 0.01m, Bottom, 0.001m]

3.4 HEC-RAS 5.0.5

HEC-RAS v. 5.0.5 is used in the analysis of the 3D surfaces. The surfaces were imported through the RAS Mapper extension in HEC-RAS. This allows for manipulation of the surfaces once imported. A two-dimensional (2D) flow area was then constructed in

the flow area. The computational grid spacing was set at 0.05 meters in the x- and y-directions. The computational time step was set at 0.1 seconds. This develops a Courant number below 2 for all of the flow conditions mentioned above and a Courant number of less than 1 for all of the low flow conditions.

3.5 Validation

Validation of a numerical model with a physical model or real-world observations is important. Validation allows for individuals to trust that what the numerical model output is showing to be correct. Numerical models are developed from lines of code and as a result, can have errors and bugs. These errors may not be noticeable unless there is a physical model to validate against. The validation information and data were determined from two research articles "Geometry of Scour Holes Associated with 90° Spur Dikes" (Kuhnle et al, 1999) and "Flow near a model spur dike with a fixed scoured bed" (Kuhnle, 2013). Both of these research articles were prepared by Roger Kuhnle in conjunction with the United States Department of Agriculture.

Table 4 shows the percent error between the physical model data and the data produced by the numerical model when it comes to incoming flow depth. This parameter was chosen because Kuhnle (1999) held the incoming flow depth constant and varied the spur dike length. "Geometry of Scour Holes Associated with 90° Spur Dikes" (Kuhnle et al, 1999) compared the length of spur dikes, channel flow rates, and scour hole geometries. A final scour hole's geometry is represented by ring-like contour lines on the channel bed as shown in Figure 8.

Table 4: Validation of Numerical Model

Spur Dike Length	Flow Conditions	Average Flow Depth (m)	Average Flow Depth (m)	Difference	% Error
Long	Low	0.186	0.1885	-0.0025	-1.34%
Long	High	0.3	0.285	0.015	5.00%
Short	Low	0.185	0.1975	-0.0125	-6.76%
Short	High	0.304	0.28	0.024	7.89%

The topographic relief map of the bed could then be inputted to Civil 3D for terrain modeling. The physical experiments were conducted in a flume located in the hydraulic laboratory at the National Sedimentation lab. The flume had an overall dimension of 30 m long, 1.2 m wide, and 0.6 m deep. Uniform-sized sand was used in all experimental runs. The sediment had a median size of 0.8 mm with a standard deviation of 1.37. Two spur dike lengths were modeled, 0.305 m and 0.152 m. The overtopping ratios were either 1.2 or 2.0 during the experiments. The experiments were continued until the changes in the scour hole became very slow, between 30 hours and 133 hours.

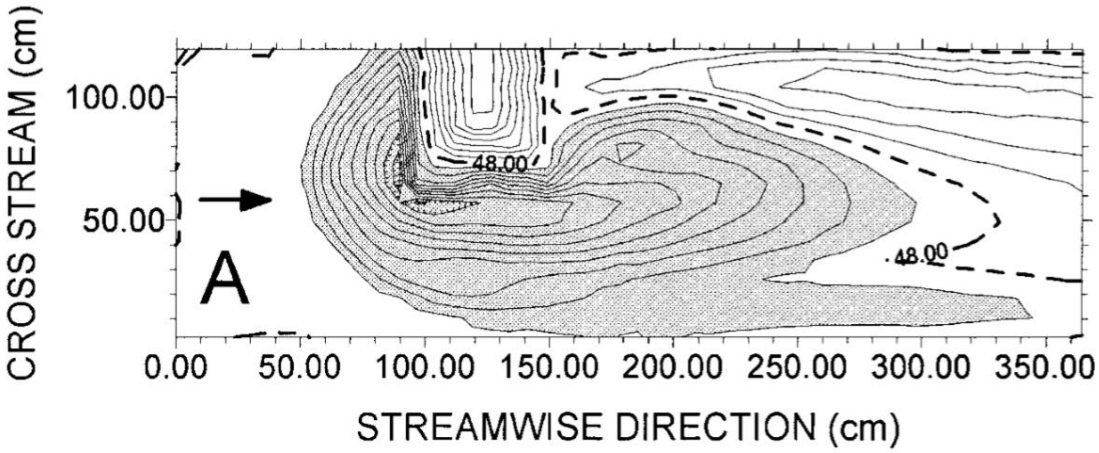

Figure 8: Topographic Scoured Bed (Kuhnle et al, 1999)

Scour hole dimension ratios were determined from the experimental runs by Kuhnle, 1999. The full table is shown in Table 2. The definition sketch of the ratios and their meaning is shown in Figure 3 in Chapter 2.

3.6 Setup

Manning's n

Manning's n of 0.037 was used throughout the analysis. Determination of a Manning's n value for any hydraulic calculation is extremely important and must be chosen with caution. Extensive research in the past has been done on the determination of Manning n values by Phillips & Tadayon (2006), Limerinos (1970), and Chow (1959.) Both Phillips and Limerinos reports were done in cooperation with the United States Geological Survey (USGS). The reports covered Manning's n determination in channelized flow as well as overbank areas. This is important to note as overbank areas normally have greatly differing roughness factors than that of the flow channel. A full Manning's n determination table is given in Appendix A from Chow (1959).

Computational Time Step & Computational Grid

The computational time step is important for efficient and stable numerical models. The initial computational time step determination may be a rough estimate with refinement done as the process moves forward. A decrease from 1 sec. to 0.5 sec. will have a doubling effect on the computational time to run the numerical model. This can greatly affect the efficiency of the model.

The other half of the computational time is the computational grid size. This size is determined within HEC-RAS and can range from as large to as small as the user would like. As with the time step, a decrease in the size of the individual grid pieces greatly

increases the computational time needed for the numerical model to complete the analysis. The length of the time step and size of the grid should be determined with the Courant number in mind. If the Courant number grows too large, the model will not produce results within the recommended error limits and may crash completely.

The Courant number was kept below a value of 2, which is recommended when using the Full Momentum equations within HEC-RAS. This was done by reducing the computational time step to 0.1 seconds with a grid size of 0.05 meters. This grid size produced a total number of cells of around 7000, depending on the model. The average run time for the model was 2 hours. As talked about earlier, if the time step was increased from 0.1 seconds to 0.3 seconds reduced the overall computation time to 45 minutes. This resulted in more warnings during the analysis though. The smaller the Courant number, the less amount of warnings and errors will be populated during analysis.

Chapter 4

4.1 Results

A summary of the dynamic outputs is shown in Table 5 and Figures 9 and 10. These outputs show the upstream flow velocity (m^3/s), upstream flow depth (m), and maximum flow velocity (m/s). All of the flow analyses are overtopping flows meaning the water overtopped the crest of the spur dike. The Run ID correlates to the earlier Run ID mentioned in Table 2. Figures 9 and 10 show the relationship between the flow fields of a long spur dike under high flow conditions with a scoured-bed (L90-3) and a flat-bed (L90-11). The location of the maximum velocity is at the crest of the spur dike in both instances. The location of maximum velocity is constant throughout all simulation analyses and can be seen in Appendix B, as well as the full velocity flow field. The maximum velocity associated with the flat-bed is higher than the scoured bed for all conditions. This allows for a relationship between the maximum velocity determined in the analysis using HEC-RAS and the maximum scour depth from overtopping flows to be developed and used accurately.

Table 5: HEC-RAS Analysis Outputs (Scoured and Flat-bed)

Run ID	Upstream Flow Velocity (m/s)	Upstream Flow Depth (m)	Maximum Flow Velocity (m/s)
L90-1	0.312	0.199	0.40
L90-2	0.335	0.178	0.44
L90-3	0.445	0.271	0.69
L90-4	0.426	0.299	0.64
S90-1b	0.315	0.192	0.42
S90-2b	0.307	0.203	0.49
S90-3	0.432	0.290	0.73
S90-4	0.460	0.270	0.65
L90-10	0.314	0.190	0.66
L90-11	0.440	0.274	0.83
S90-10	0.315	0.190	0.66
S90-11	0.458	0.271	0.69

The geometry of the scoured-beds (L90-1 – L90-4, S90-1b – S90-4) is shown in Appendix B as well.

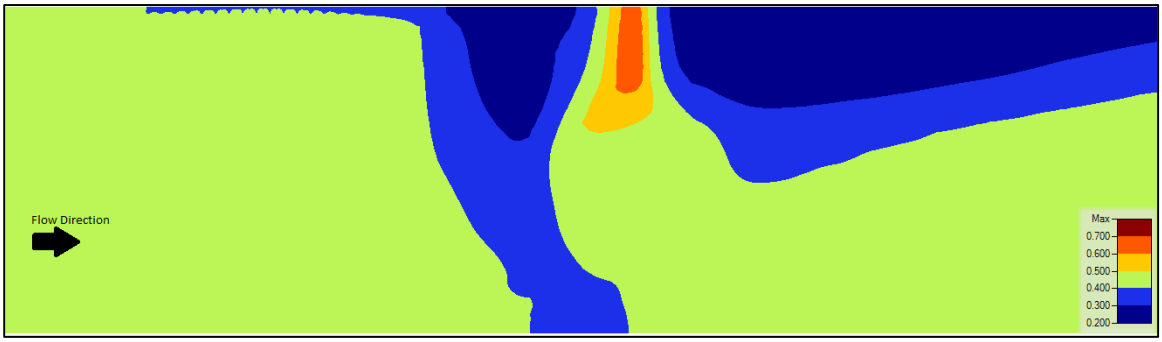

Figure 9: Flow Velocity Field (Run ID: L90-3)

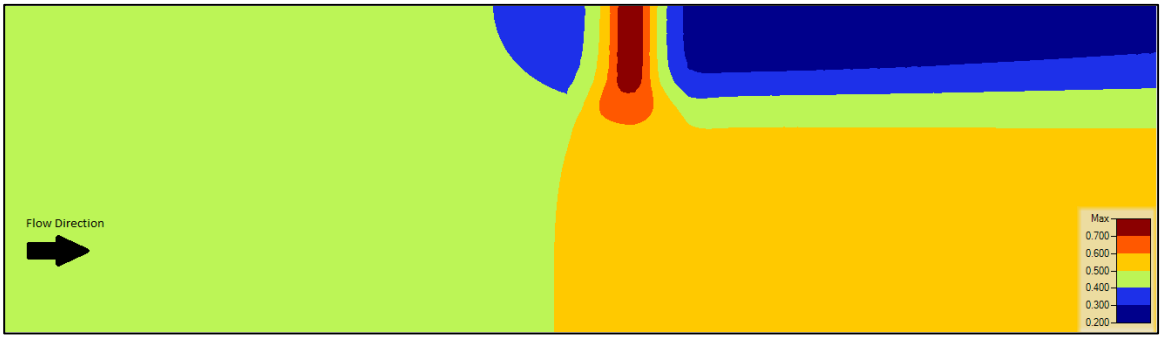

Figure 10: Flow Velocity Field (Run ID: L90-11)

Correlation

A correlation analysis was performed with Minitab statistical analysis software to determine which of the parameters measured by Kuhnle et al, 1999 are one-to-one correlated. The parameter correlation is shown in Figure 11. From the statistical analysis, it was determined that the maximum scour depth and maximum scour volume are correlated to the spur dike length and the Froude number as can be seen in Figure 11. This correlation makes sense, as the contraction of the flow cross-section by an increase in spur dike length, increases flow velocities in the channel and thus increases the erosive capabilities of the flow. The Froude number is a dimensionless parameter that associates the velocity of the flow and the hydraulic depth of the flow cross-section along with gravity forces, with an increase in velocity or decrease in hydraulic depth, there is an increased capacity for erosion and development of scour holes. It was also found that the Froude number is correlated with the Shear Velocity and Shear Velocity Ratio. This correlation means that an increase in Froude number directly affects the erosive capabilities of flow. As well as, the shear velocity and shear velocity ratio having a secondary correlation with the maximum scour depth and maximum scour velocity.

The remaining variables were determined to be uncorrelated individually with the scour depth and scour volume. These include upstream flow depth, flow rate, and overtopping ratio.

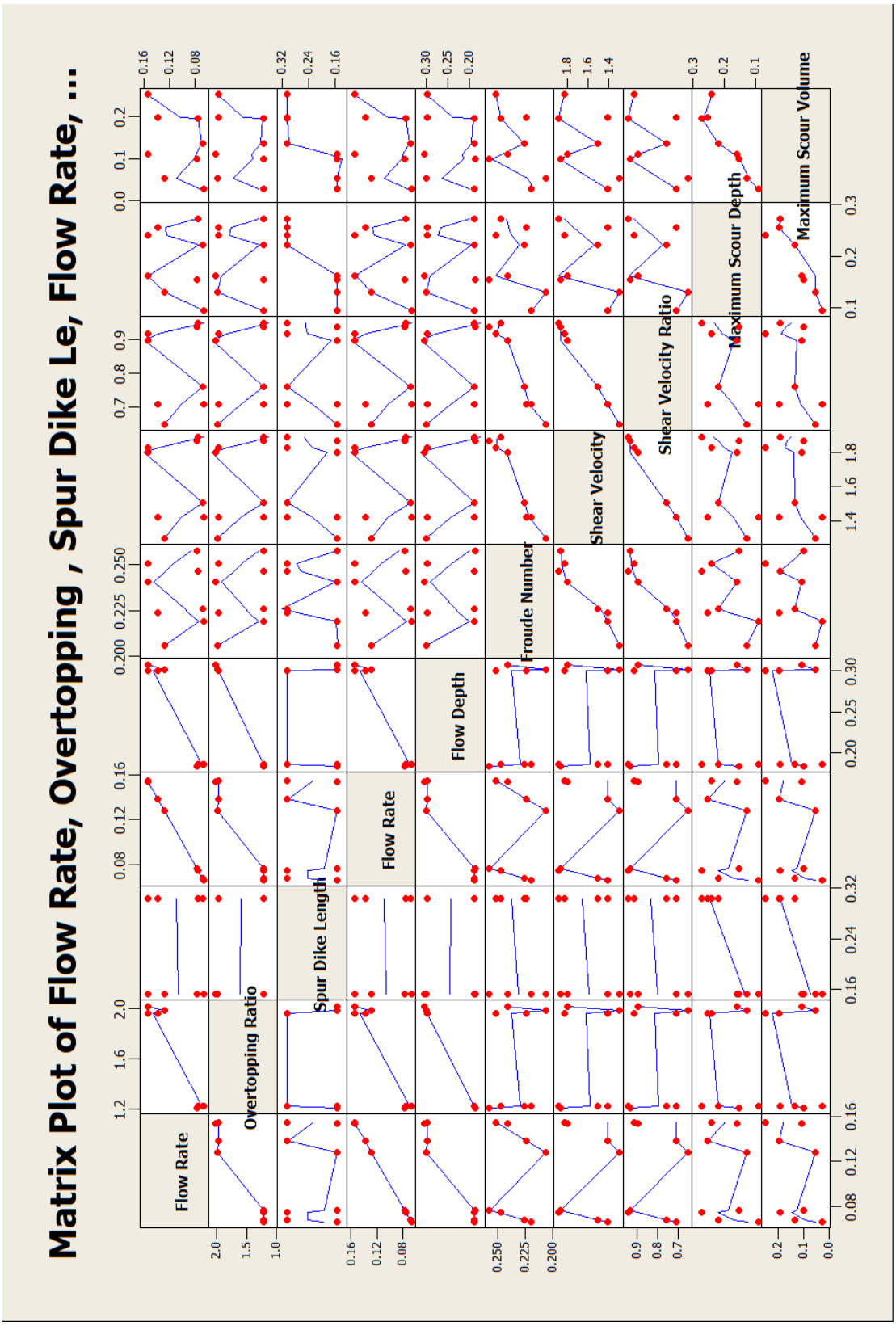

Figure 11: Minitab's Matrix Plot for Correlation of Parameters

4.2 Discussion

Comparison

All flows analyzed are overtopping flows. This condition normally occurs during peak flow and flooding events. Spur dikes cannot normally be built to reduce the chance of overtopping to zero, as this would mean the spur dike would need to reach the same height as the top of the bank. This situation is normally uneconomical for the benefit received by the implementation of spur dikes at this height. The maximum scour depth occurred at the leading edge of the spur dike. A second scour hole forms downstream of the spur dike with the increase from 0.152m to 0.305m in the length of the spur dike. The dynamic variables are shown in Tables 6 and 7. These dynamic variables were taken from the HEC-RAS 2D analysis outputs.

Table 6: Comparison of Dynamic Variables (Scoured Bed)

Run ID	Ratio of V_{max}/V_1	Froude #	Ratio of V_{max}/Froude #	Maximum Scour Depth (m)
L90-1	1.282	0.223	1.791	0.24
L90-2	1.313	0.254	1.736	0.2
L90-3	1.555	0.273	2.536	0.22
L90-4	1.502	0.249	2.573	0.27
S90-1b	1.337	0.230	1.834	0.12
S90-2b	1.593	0.218	2.248	0.08
S90-3	1.681	0.256	2.835	0.11
S90-4	1.417	0.283	2.307	0.12

Channel Flow Rates

As shown in Table 7, the ratio of V_{max}/V_1 and the Froude number (Fr #) seem to be inversely related to one another for the flat-bed scenario. As the Fr # increases with an increase in flow rate, the V_{max}/V_1 decreases. An increase in channel flow rate does not

Table 7: Comparison of Dynamic Variables (Flat-bed)

Run ID	Ratio of V_{max}/V_1	Froude #	Ratio of V_{max}/Froude #
L90-10	2.092	0.230	2.857
L90-11	1.886	0.268	3.093
S90-10	2.092	0.231	2.856
S90-11	1.507	0.281	2.456

necessarily correlate to an increase in maximum scour depth. Conversely, the scoured bed trials show a correlation between the V_{max}/V_1 and the Fr #. This could show that when V_{max}/V_1 and the Fr # vary inversely, that the bed has the potential to be scoured during flow. Then, when the V_{max}/V_1 and the Fr # vary in unison, it shows that the bed has reached stability. The maximum scour depth for the low flow conditions averaged at 0.16 m, the high flow conditions averaged at 0.18 m. While there is a slight increase in the average depth, it is negligible when compared with other factors for scour depth. Table 8 shows the relationship between flow conditions and maximum scour depth.

Table 8: Comparison of Flow Conditions and Maximum Scour Depth

Run ID	Flow (m^3/s)	Maximum Scour Depth (m)	Average Depth (m)
L90-1	0.072	0.24	
L90-2	0.072	0.2	
S90-1b	0.072	0.12	
S90-2b	0.072	0.08	0.160
L90-3	0.144	0.22	
L90-4	0.144	0.27	
S90-3	0.144	0.11	
S90-4	0.144	0.12	0.180

Length of Spur Dike

A change in the length of the spur dike correlates directly to the maximum scour depth as shown in Figure 11: Minitab's Matrix Plot for Correlation of Parameters. A longer spur dike intrudes further into the flow field and thus reducing the flow area. This reduction in flow area causes an increase in flow velocity through the reduced flow area causing an increase in scour ability. This is shown directly in the data and should be noted that an increase in spur dike length has a greater effect on the depth of scouring than does an increase in flow rate. Table 9 shows the relationship between the short and long spur dikes with the maximum scour depth. The average maximum scour depth increases from 0.108 m for short spur dikes to 0.233 m for long spur dikes.

Table 9: Comparison of Length of Spur Dike and Maximum Scour Depth.

Run ID	Length (m)	Maximum Scour Depth (m)	Average Depth (m)
L90-1	0.305	0.24	
L90-2	0.305	0.2	
L90-3	0.305	0.22	
L90-4	0.305	0.27	0.233
S90-1b	0.152	0.12	
S90-2b	0.152	0.08	
S90-3	0.152	0.11	
S90-4	0.152	0.12	0.108

Predicting Scour Hole Depth

Melville (1992) determined the equation, shown in Equation 22, for use with bridge abutments. Bridge abutments are similar to spur dikes in shape and hydraulic design

requirements. Much of the data and experimentation has been used to cross over between bridge abutments and spur dikes in design guidelines.

$$\frac{d}{Y} = 2K_M\eta^{(1-\delta)} \quad (22)$$

The Melville equation was developed by using laboratory data with all flow depths being less than the height of the structure (Kuhnle et al, 1999). Kuhnle (1999) used laboratory experimentation to determine the accuracy of the equation when using overtopping flows on spur dike analysis. Kuhnle (1999) theorized that the equation could be manipulated to calculate scour depths during higher flows, as well as the lower flows are shown by Melville (1992). Kuhnle (1999) determined that the mean value of the ratio of measured to calculated scour depths for the data was 0.56 for the overtopping flows. Thus Kuhnle (1999) modified the Melville equation to the following equation shown in Equation 23.

$$\frac{d}{Y} = 1.12K_M\eta^{(1-\delta)} \quad (23)$$

This accounts for the 0.56 discrepancy by multiplying the leading coefficient (2) by 0.56 to get the new coefficient (1.12). This transformation of the Melville (1992) equation shows the continued importance of the factors included in determining the maximum scour depth (d) in both regular and overtopping flow conditions. These factors include the incoming flow depth (Y), the ratio of the length of spur dike to incoming flow depth (η), and the power function (δ, which is a function of η). Equation 24 shows the Froude-Adjusted equation developed in this research.

$$\frac{d}{Y} = 0.14K_M\eta^{(1-\delta)} \quad (24)$$

Due to the ease of determining upstream flow and maximum flow velocities, as well as flow depth, from the HEC-RAS output, a ratio of $V_{max}/V_1 = V_r$ will be used to determine the K_M value, instead of U/U_c (shear velocity ratio) used by Kuhnle (1999). The K_M value will be determined from V_r/Fr_1 (Fr_1 = approach Froude number). This will allow for a depth of scour to be estimated without the need for a physical model. Physical models take time and money to build and even then, they are only suitable for the particular instance where they were designed for. A numerical model can be changed with the ease of a computer, is time-saving, and money-saving option to the costly physical models. The leading coefficient was changed to 0.14 to allow for the change in K_M factors. Figure 12 shows the measured and predicted scour depths from HEC-RAS as well as from Kuhnle (1999) predicted scour depths. The resulting formula is shown in Equation 24.

The predicted scour depths based on $K_M = V_r/Fr_1$ (Froude-Adjusted) method are closer to the measured scour depths than the Kuhnle (1999) Modified Melville equation. The Modified Melville equation over predicts the depth of scour by an average of 14%, while the Froude-Adjusted Melville equation under predicts by 1%. If the absolute error is taken, the Modified Melville error remains the same but the Froude-Adjusted error increases to 7%. This is due to the negative error during two analyses. The predicted and measured scour depths along with the errors by each are shown in Table 10.

The Froude-adjusted model works better overall but has extremely less error in the long spur dike runs. The short spur dikes seem to have more variability in the scour depths. The scour depth may be affected by a different parameter that does not affect the long spur dike scour depth. This could be due to the limited extent that the spur dike protrudes into the channel. As the length of spur dike to channel width (L/T) increases, the scour depth becomes larger.

Table 10: Predicted and Measured Scour Depths

Run ID	Predicted Modified Melville	Predicted Froude-Adjusted	Measured Scour Depth	Difference Modified Melville	% Error Modified Melville	Difference Froude-Adjusted	% Error Froude-Adjusted
L90-10	0.227	0.221	0.220	0.007	3.1%	0.001	0.3%
L90-11	0.277	0.238	0.245	0.032	11.5%	-0.007	-2.9%
S90-10	0.141	0.115	0.100	0.041	29.2%	0.015	12.7%
S90-11	0.133	0.101	0.115	0.018	13.5%	-0.014	-13.9%
				Avg. Error	14%		-1%

Predicting Scour Hole Volumes

Kuhnle (1999) developed a relationship between the depth of scour, length of spur dike, and the incoming flow depth for determining the volume of a scour hole. This relationship is shown in Equation 25.

$$\frac{V_{30}}{(d_{30})^3} = 17.106\left(\frac{L}{Y}\right)^{-0.781} \quad (25)$$

This relationship was checked against the measured scour hole volumes produced in the flume experiments. The discrepancy ratio (predicted/measured) for the volume of scour ranged from 0.783 to 1.486 (Kuhnle et al, 1999).

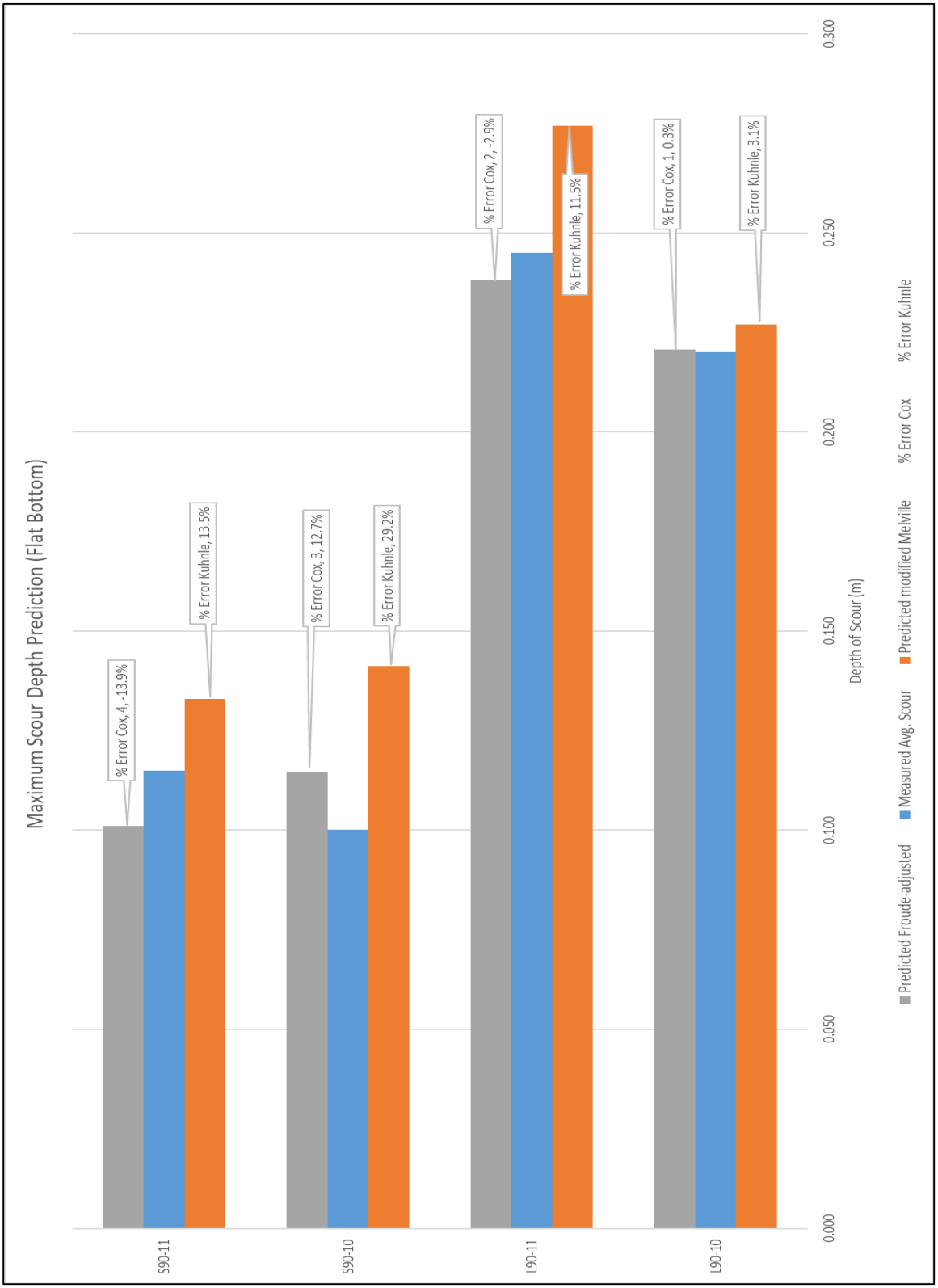

Figure 12: Comparison of Predicted and Measured Scour Depths (% Error from Measured values shown in callouts)

The maximum scour depths were computed using the Froude-Adjusted maximum scour depths. The comparison of Modified-Melville and Froude-Adjusted scour volumes against the measured scour volumes is shown in Table 11.

Table 11: Predicted and Measured Scour Hole Volumes

Run ID	Modified Melville	Froude-Adjusted Melville	Measured Value	% Error - Modified Melville	% Error - Froude Adjusted
L90-10	0.1384	0.1271	0.1646	-19%	-30%
L90-11	0.3339	0.2126	0.2247	33%	-6%
S90-10	0.0574	0.0306	0.0628	-9%	-105%
S90-11	0.0632	0.0277	0.0808	-28%	-192%

The large increase in error from the Modified-Melville to the Froude-Adjusted may be due to the fact that the scour hole volume equation (25) was developed to work directly with the Modified-Melville outputs and optimized for that purpose.

Anomalies

It was determined that for low slope areas, the Eddy Viscosity Coefficient can be left to the default value of 0. This is due to the negligible effect of turning the coefficient on, coupled with the dramatic increase in run time for the analysis. The Eddy Viscosity Coefficient should be turned on when the velocity in the channel system reaches above 2.5 ft/s. This seems to be the threshold for the Full Momentum equation to correctly model an eddy without the need for the Eddy Viscosity Coefficient.

It should also be noted that HEC-RAS ran stably with a Courant Number as high as 18. Even with recommendations for keeping the Courant Number below 3, if possible. This shows that the Courant Number should only be of concern if the water velocities are

quite high or the terrain is highly irregular and thus will cause the analysis to crash. Also, the Courant number should be revisited during final design checks, as a high Courant number was shown to overestimate the maximum velocity in the channel.

Large sediment deposition occurred downstream of the scour hole shown in the topographic relief given by Kuhnle (1999). This could have a large effect on the downstream flow regime and the possible location of more spur dikes.

4.3 Procedure for Determining Scour Depth

The following procedure was used to determine the maximum scour depth.

1. Obtain flow characteristic data (flow depth, flow rate, flow velocity)
2. Obtain bathymetry/DEM and slope data
3. Obtain validation data for later use
4. Input parameters into HEC-RAS
5. Validate existing conditions analysis against measured data
6. Determine spur dike parameters (length, width, height, angle)
7. Input spur dike data to channel bathymetry
    a. Use Civil3D
8. Perform analysis on proposed surface
9. Determine maximum velocity and incoming flow depth in channel
10. Use Froude-adjusted Melville (Eq. 24) to determine maximum scour depth
11. Adjust spur dike parameters if maximum scour depth is unacceptable

Chapter 5

5 Conclusion

The determination of the depth of maximum scour is extremely important to the design of a hydraulic structure. Inadequate scour design leads to failure of hydraulic structures. Being able to design hydraulic structures without the need for physical models will help propel the design process forward at an accelerated rate. This is important for the timely and cost-effective design and construction of hydraulic structures.

Developing a simple procedure to effectively determine the maximum scour for a HEC-RAS 2D analysis has been shown to be accurate in this research. The adaptation of existing empirical equations allows for a proven technique to be used with current technology. The interactions between the upstream flow depth, the maximum channel velocity, length of spur dike, and upstream flow velocity are easily attained from the HEC-RAS 2D analysis output. This will allow for ease of determining the depth of scour for the given spur dike setup.

The Froude-number adjusted Melville equation to be used with HEC-RAS 2D outputs reduced the average error in determining the maximum scour depth from 14% to -1%. This reduction in error will allow for an increase in accuracy and efficiency in design. The estimation of scour hole volume increased in average error from -6% to -83% from

the Modified-Melville to the Froude-Adjusted equation. This may be due to the fact that the scour hole volume equation (25) was developed for use with the Modified-Melville equation.

The largest limitation in this research is the lack of physical modeling data on scour holes developed by spur dikes. The introduction of more physical data could allow for greater accuracy in determining the maximum scour depth.

Chapter 6

6 Further Research Needed

Further research needs to be done on the effect of spacing multiple spur dikes on the maximum scour depth. Introducing multiple spur dikes could lead to lower levels of scour and increased protection of the bank. There has been limited research done in this area. One of the complications with bringing in more factors is the increase in the number of analyses that need to be performed to accurately model all contributing factors.

Also, the effect of different soil types on the scour depths needs to be further researched. As soil becomes finer, there is a higher chance for erosion and scour but to what degree is unknown. This is an area that will need further research as most channel beds are not uniform in soil type and range from one to the next.

A deeper look into the estimation of scour hole volumes based on a modified version of the equation that Kuhnle proposed will be needed to accurately estimate the volume. This will need to be done in future research. Along with the inclusion of more lengths of spur dikes and flow regimes to better define the maximum scour depth. This will need to involve a physical model, as well as a numerical model to study and develop relationships across multiple designs.

References

Allen, J.R.L. (1985). “Principles of Physical Sedimentology.” *George Allen & Unwin*, Herts, United Kingdom.

AUTODESK. Civil 3D. Computer software. Vers. 2019. AutoCAD Civil 3D. 2019. 2019. <https://www.autodesk.com/products/civil-3d/overview>

Baird, D.C., Lotherby, L., Klumpp, C.C., Scurlock, S.M. (2015). “Bank Stabilization Design Guidelines.” *U.S. Department of the Interior: Bureau of Reclamation.* SRH-2015-25.

Bhuiyan, F., Hey, R.D., Wormleaton, P.R. (2010). “Bank-Attached Vanes for Bank Erosion Control and Restoration of River Meanders.” *Journal of Hydraulic Engineering.* 136 (9), 583-596.

Biedenharn, D.S., Watson, C.C. (1997). “Stage adjustment in the Lower Mississippi River, USA.” *Regulated Rivers: Research and Management.* 13 (6), 517-536.

Biglari, B., Strum, T.W. (1998). “Numerical modeling of flow around bridge abutments in compound channel.” *Journal of Hydraulic Engineering.* 124 (2), 156-164.

Brunner, G. (2016). “HEC-RAS River Analysis System, 2D Modeling User’s Manual Version 5.0.” *US Army Corps of Engineers Institute for Water Resources.* CPD-68A.

Burguete, J., Garcia-Navarro, P., Murillo, J. (2008). “Friction term discretization and limitation to preserve stability and conservation in the 1D shallow-water model: application to unsteady irrigation and river flow.” *International Journal of Numerical Methods Fluids.* 58 (4), 403-425.

Cao, X., Gu, Z., Tang, H. (2013). “Study on Spacing Threshold of Nonsubmerged Spur Dikes with Alternate Layout.” *Journal of Applied Mathematics.* vol. 2013, Article ID 945984, 8 pg.

Chang, K-H., Sheu, T., Chang, T-J. (2018). “A 1D-2D coupled SPH-SWE model applied to open channel flow simulations in complicated geometries.” *Advances in Water Resources.* 115, 185-197.

Chen, L-P., Jiang, J-C. (2010). “Experiments and numerical simulations on transport of dissolved pollutants around spur dike.” *Water Science and Engineering.* 3, 341-353.

Chow, V.T. (1959). “Open-Channel Hydraulics.” New York, McGraw-Hill

Copeland, R.R, (1983). “Bank Protection Techniques using Spur Dikes.” *U.S. Army Engineer Waterways Experiment Station, Hydraulics Laboratory.* 83-03-02-013

Duan, J.G., He, L., Fu, X., Wang, Q. (2009). “Mean flow and turbulence around experimental spur dike.” *Advances in Water Resources.* 32, 1717-1725

Fazli, M., Ghodsian, M., Neyshabouri, S.A.A.S. (2008). "Scour and flow field around a spur dike in a 90° bend." *International Journal of Sediment Research.* 23, 56-68.

Fazli, M., Ghodsian, M., Neyshabouri, S.A.A.S. (2007). "An experimental investigation on scour around sur dikes located at different positions in a 90 degree of bend." *32nd IAHR Congress.* Venice.

Garde, R.J. (2012). "River Morphology." *New Age International Publishers,* New York.

Ghodsian, M., Vaghefi, M. (2009). "Experimental study on scour and flow field in a scour hole are a T-shape spur dike in a 90-degree bend." *Flow Measurement Instrumentation.* 21, 292-298.

Giglou, A.N., Mccorquodale, J.A., Solari, L. (2017) "Numerical study on the effect of the spur dikes on sedimentation pattern."*Ain Shams Engineering Journal.* (Article in Press)

Heintz, M.L. (2002). "Investigation of bendway weir spacing." M.S. Thesis. Colorado State University, Department of Civil Engineering. Fort Collins, Colorado.

Hsu, M.H., Fu, J.C., Liu, W.C. (2003). "Flood routing with real-time stage correction method for flash flood forecasting in the Tanshui River, Taiwan." *Journal of Hydrology.* 283 (1-4), 267-280.

Krishna, P.S., Indulekha, K.P., Balan, K. (2015). "Analysis of groyne placement on minimizing riverbank erosion" *International Conference on Emerging Trends in Engineering, Science, and Technology.* 24, 47-53.

Kuhnle, R., Alsonso C. (2013). "Flow near a model spur dike with a fixed scoured bed." *International Journal of Sediment Research.* 28, 349-357.

Kuhnle, R., Alsonso, C., Shields, F.D.Jr. (1999). "Geometry of Scour Holes Associated with 90° Spur Dikes." *Journal of Hydraulic Engineering*. 125(9), 972-978.

Lagasse, P.F., Clopper, P.E., Pagan-Ortiz, J.E., Zevenbergen, L.W., Arneson, L.A., Chall, J.D., Girard, L.G. (2009). "Bridge Scour and Stream Instability Countermeasures: Experience, Selection, and Design Guidance." *Federal Highway Administration, Arlington, VA.* FHWA Rep. No. NHI-09-12, HEC-23, 3rd Ed, Vol. 2.

LeVeque, R. (2002). "Finite Volume Methods for Hyperbolic Problems." *Cambridge Texts in Applied Mathematics, Cambridge University Press.*

Limerinos, J.T. (1970). "Determination of the Manning Coefficient From Measured Bed Roughness in Natural Channels." *United States Geological Survey, Studies of Flow in Alluvial Channels.* Water-Supply Paper 1898-B.

Lintott, C. (2017). "HEC-RAS 2D – An Accessible and Capable Modeling Tool." *Water New Zealand's 2017 Storm water Conference.*

Melville, B.W. (1992). "Local Scour at Bridge Abutments." *Journal of Hydraulic Engineering.* 118 (4), 615-631.

Mohammad, V., Yaser, S., Shaker, H.S. (2015). “Effects of distance between the T-shaped spur dikes on flow and scour patterns in 90° bend using the SSIIM model.” *Ain Shams Engineering Journal.* 7, 31-45.

Phillips, J.V., Tadayon, S. (2006). “Selection of Manning’s Roughness Coefficient for Natural and Constructed Vegetated and Non-vegetated Channels, and Vegetation Maintenance Plan Guidelines for Vegetated Channels in Central Arizona.” *United States Geological Survey, Scientific Investigation Report*. 2006-5108.

Prasad, K.S., Indulekha, K.P., Balan, K. (2015). “Analysis of groyne placement on minimising riverbank erosion.” International Conference on Emerging trends in Engineering, Science and Technology. 24, 47-53.

Przedwojski, B. (1995). “Bed topography and local scour in rivers with banks protected by groynes.” *Journal of Hydraulic Restoration.* 33 (2), 257-273.

Scurlock, S.M., Cox, A.L., Thornton, C.I., Abt, S.R. (2012). “Transverse instream structure analysis: Maximum and average velocity ratios within the prismatic channel.” *Bureau of Reclamation, Denver Technical Service Center*.

Sturm, T.W. (2009) “Open Channel Hydraulics.” McGraw-Hill Education, United States, ISBN13: 9780073397870

Unami, K., Kawachi, T., Bahar, M.M., Itagaki, H. (1999). “Two-dimensional numerical model of spillway flow.” *Journal of Hydraulic Engineering*. 125 (4), 369-375.

US. Army Corp of Engineers. HEC-RAS. Computer software. Vers. 5.0.5. US Army Corps of Engineers – Hydrologic Engineering Center. 2018. 2019 <https://www.hec.usace.army.mil/software/hec-ras/>

U.S. Army Corp of Engineers. HEC-RAS. Computer software. Vers. 5.0.7. US Army Corps of Engineers – Hydrologic Engineering Center. 2019. 2019 <https://www.hec.usace.army.mil/software/hec-ras/>

Ying, Q., Jiao, Z.B. (2004) “Hydraulics of Spur Dike” Ocean Press, Beijing, China.

Ying, X.Y., Khan, A.A., Wang, S.S.Y. (2004) “Upwind conservative scheme for the Saint Venant Equations.” *Journal of Hydraulic Engineering.* 130 (10) 977-987.

Appendix A

Data

Manning's n for Channels (Chow, 1959).

Type of Channel and Description	Minimum	Normal	Maximum
Natural streams - minor streams (top width at floodstage < 100 ft)			
1. Main Channels			
a. clean, straight, full stage, no rifts or deep pools	0.025	0.030	0.033
b. same as above, but more stones and weeds	0.030	0.035	0.040
c. clean, winding, some pools and shoals	0.033	0.040	0.045
d. same as above, but some weeds and stones	0.035	0.045	0.050
e. same as above, lower stages, more ineffective slopes and sections	0.040	0.048	0.055
f. same as "d" with more stones	0.045	0.050	0.060
g. sluggish reaches, weedy, deep pools	0.050	0.070	0.080
h. very weedy reaches, deep pools, or floodways with heavy stand of timber and underbrush	0.075	0.100	0.150
2. Mountain streams, no vegetation in channel, banks usually steep, trees and brush along banks submerged at high stages			
a. bottom: gravels, cobbles, and few boulders	0.030	0.040	0.050
b. bottom: cobbles with large boulders	0.040	0.050	0.070

Inputs for Analysis (Table 2)

Run ID	Flow (m^3/s)	Length (m)	Manning's n	Computational Grid Spacing (m)	Computational Time Step (s)
L90-1	0.072	0.305	0.037	0.05	0.1
L90-2	0.072	0.305	0.037	0.05	0.1
L90-3	0.144	0.305	0.037	0.05	0.1
L90-4	0.144	0.305	0.037	0.05	0.1
S90-1b	0.072	0.152	0.037	0.05	0.1
S90-2b	0.072	0.152	0.037	0.05	0.1
S90-3	0.144	0.152	0.037	0.05	0.1
S90-4	0.144	0.152	0.037	0.05	0.1

Outputs from Analysis (Table 3)

Run ID	Upstream Flow Velocity (m/s)	Upstream Flow Depth (m)	Maximum Flow Velocity (m/s)	Courant Number	Froude #	Overtopping Ratio
L90-1	0.312	0.199	0.40	0.800	0.223	1.31
L90-2	0.335	0.178	0.44	0.880	0.254	1.17
L90-3	0.445	0.271	0.69	1.384	0.273	1.78
L90-4	0.426	0.299	0.64	1.280	0.249	1.97
S90-1b	0.315	0.192	0.42	0.842	0.230	1.26
S90-2b	0.307	0.203	0.49	0.978	0.218	1.34
S90-3	0.432	0.290	0.73	1.452	0.256	1.91
S90-4	0.46	0.270	0.65	1.304	0.283	1.78

Comparison Data

Run ID	Ratio of V_{max}/V_1	Froude #	Ratio of V_{max}/Froude #	Maximum Scour Depth (m)
L90-1	1.282	0.223	1.791	0.24
L90-2	1.313	0.254	1.736	0.2
L90-3	1.555	0.273	2.536	0.22
L90-4	1.502	0.249	2.573	0.27
S90-1b	1.337	0.230	1.834	0.12
S90-2b	1.593	0.218	2.248	0.08
S90-3	1.681	0.256	2.835	0.11
S90-4	1.417	0.283	2.307	0.12

Scour Hole Maximum Depth (Predicted & Measured)

Run ID	Predicted modified Melville	Predicted Froude-adjusted	Measured Scour Depth	Difference Kuhnle	% Error Kuhnle	Difference Cox	% Error Cox
L90-10	0.227	0.221	0.220	0.007	3.1%	0.001	0.3%
L90-11	0.277	0.238	0.245	0.032	11.5%	-0.007	-2.9%
S90-10	0.141	0.115	0.100	0.041	29.2%	0.015	12.7%
S90-11	0.133	0.101	0.115	0.018	13.5%	-0.014	-13.9%
				Avg. Error	14%		-1%

Scour Hole Volumes (Predicted & Measured)

Run ID	Modified Melville	Froude-Adjusted Melville	Measured Value	% Error - Modified Melville	% Error - Froude Adjusted
L90-10	0.1384	0.1271	0.1646	-19%	-30%
L90-11	0.3339	0.2126	0.2247	33%	-6%
S90-10	0.0574	0.0306	0.0628	-9%	-105%
S90-11	0.0632	0.0277	0.0808	-28%	-192%
			Average Error	-6%	-83%

Appendix B

Screenshots

Scour Hole Relief Maps (Kuhnle et al 1999)

Run ID: S90-1b

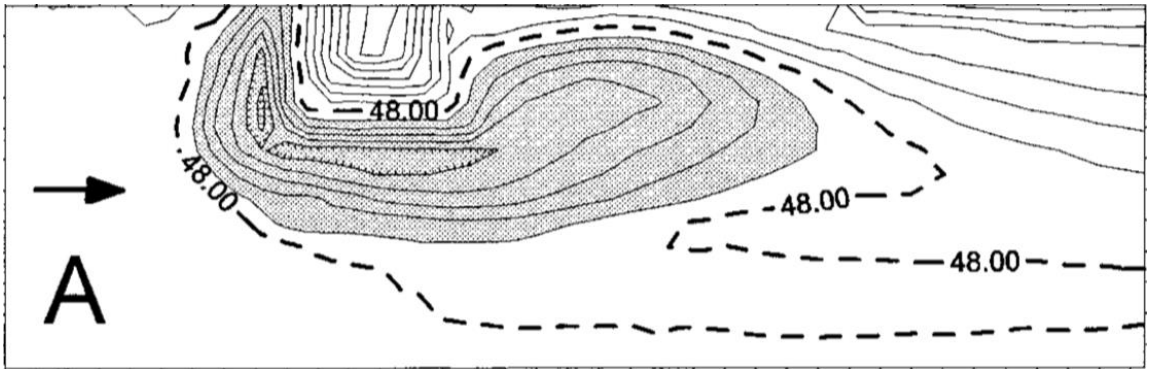

Run ID: S90-4

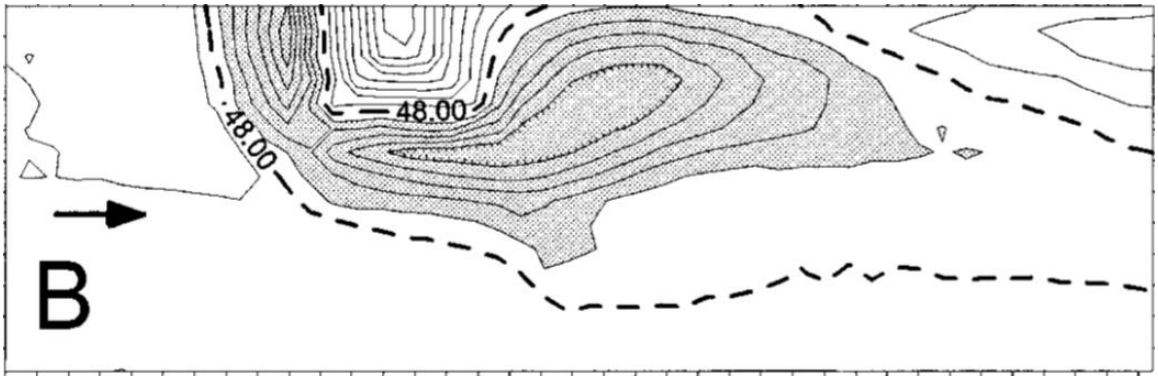

Run ID: L90-2

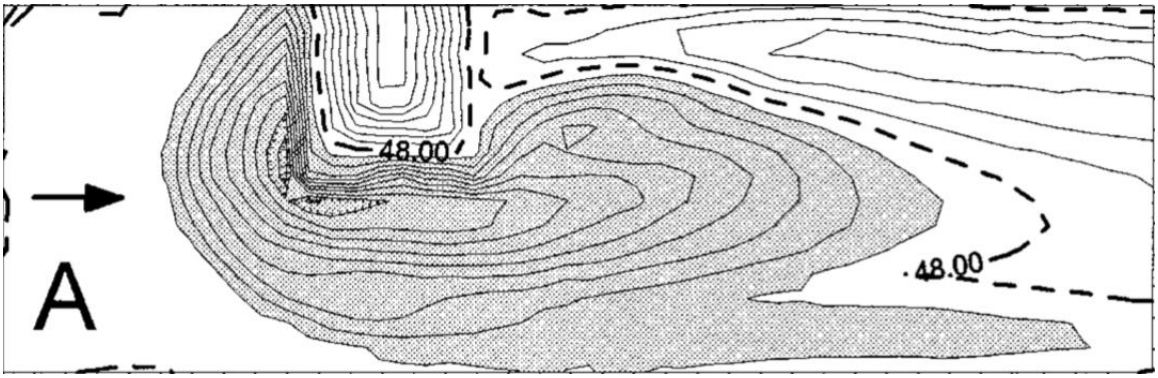

Run ID: L90-3

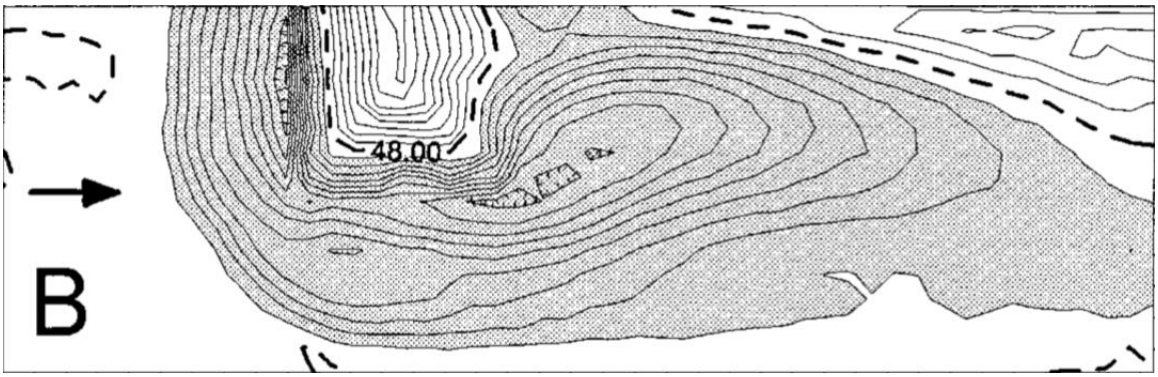

Runs: S90-2b, S90-3, L90-1, and L90-4 no relief map supplied, data extracted directly from survey data.

Civil 3D Surfaces

Run ID: S90-1b

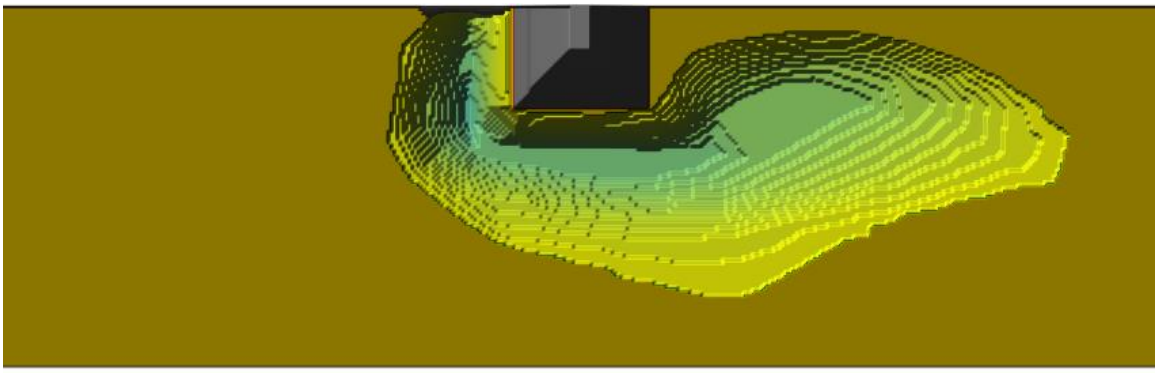

Run ID: S90-2b

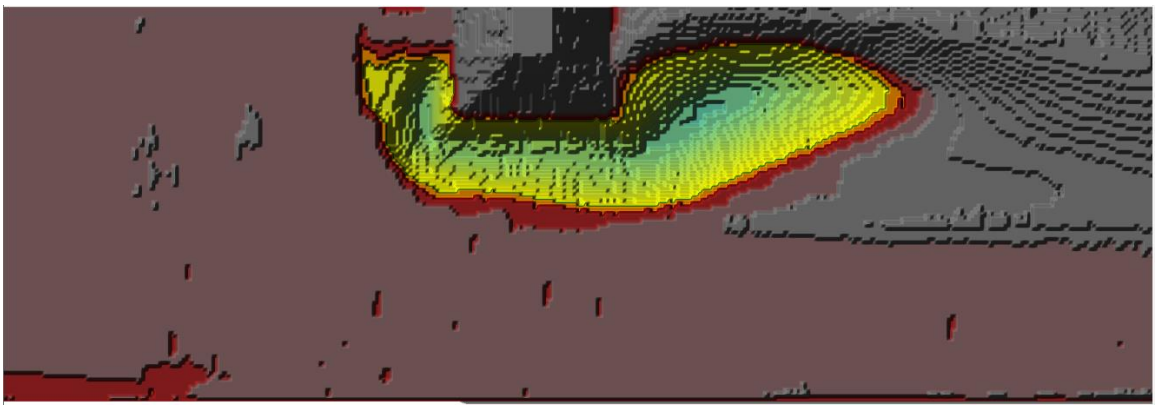

Run ID: S90-3

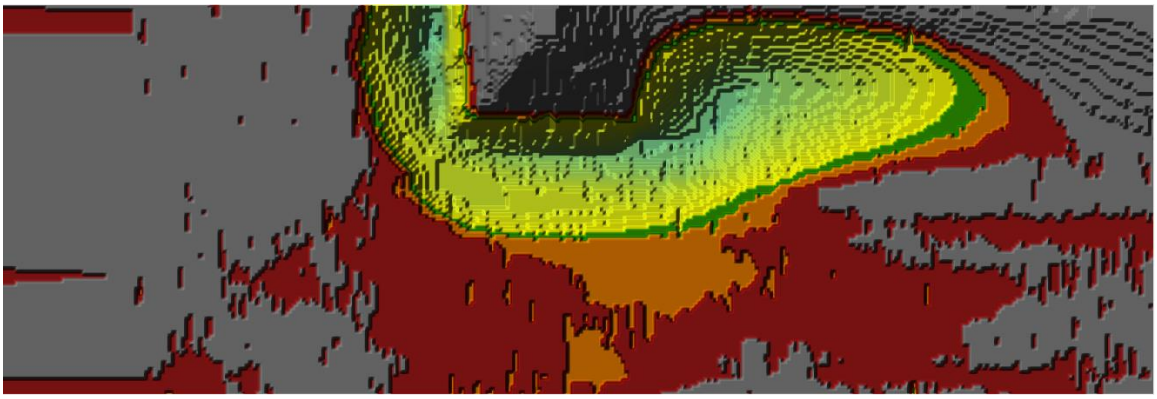

Run ID: S90-4

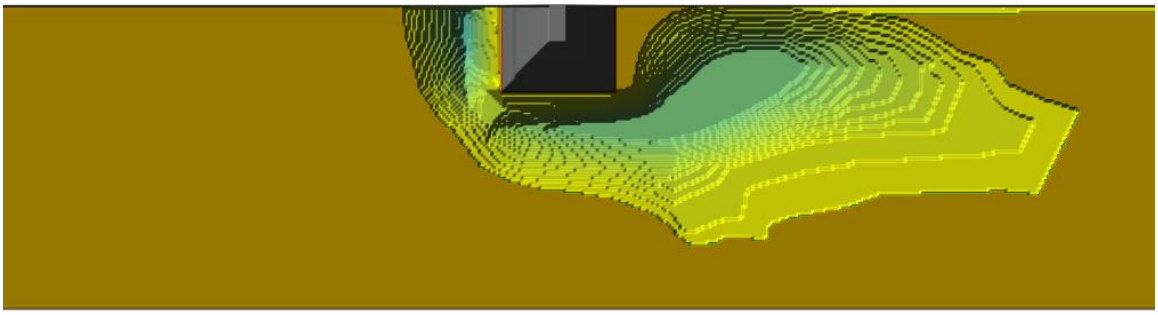

Run ID: L90-1

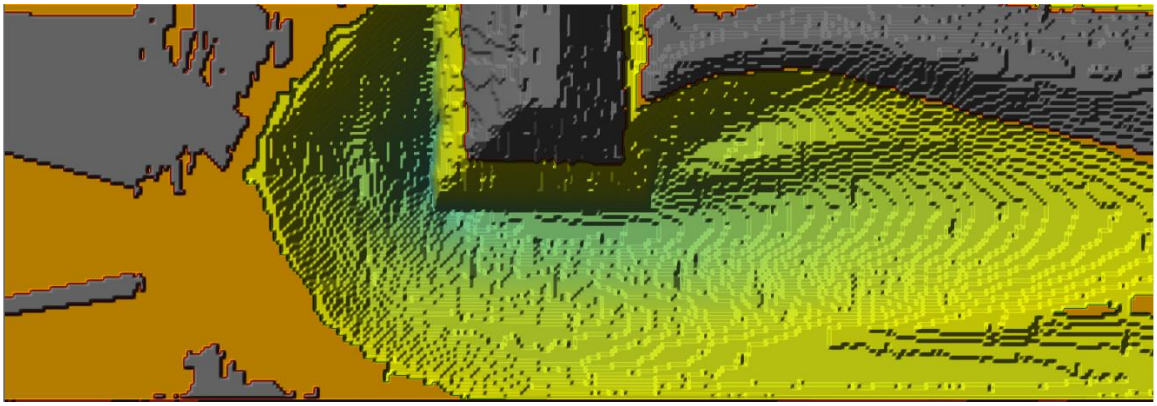

Run ID: L90-2

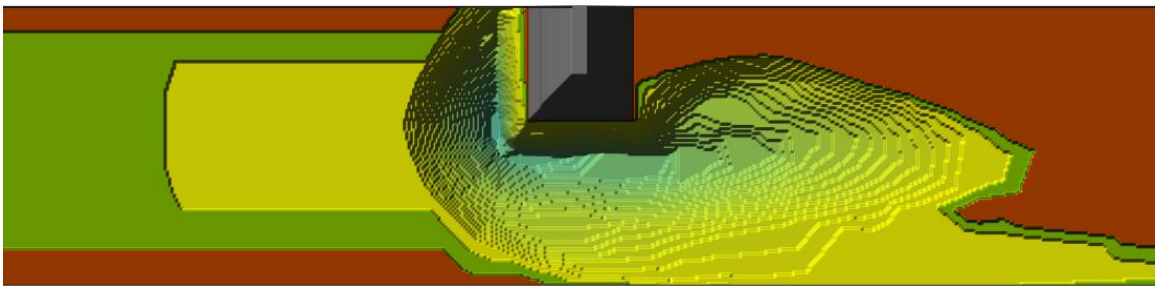

Run ID: L90-3

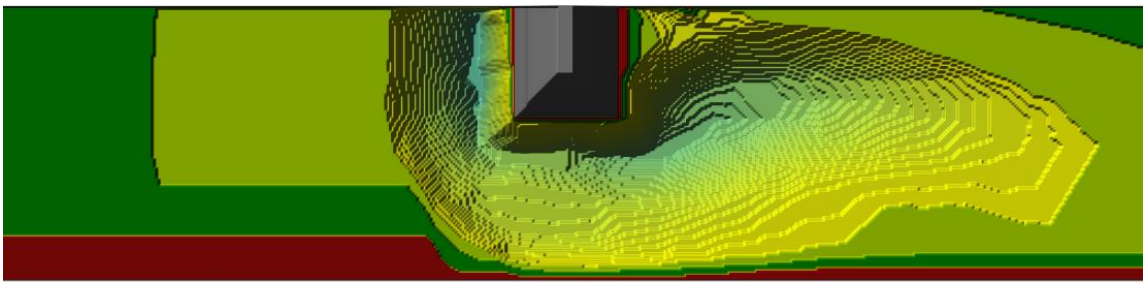

Run ID: L90-4

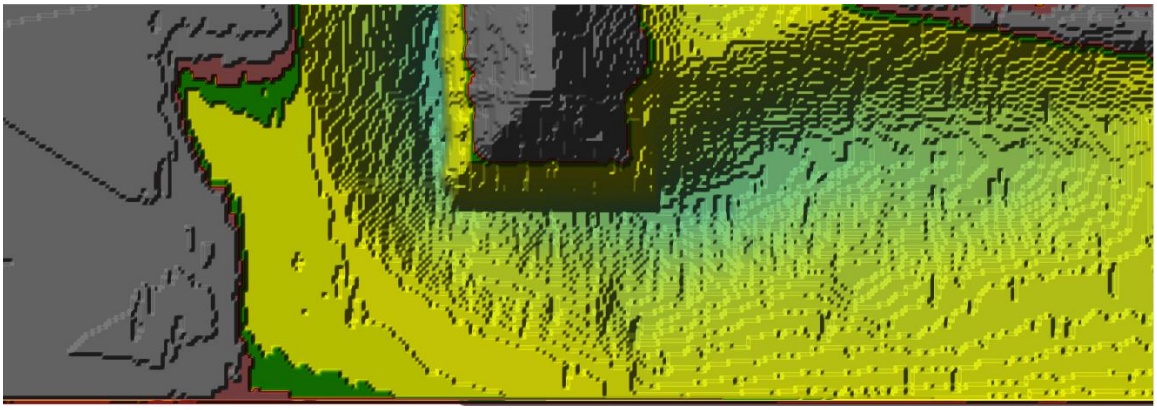

Run ID: L90-10 & L90-11

Run ID: S90-10 & S90-11

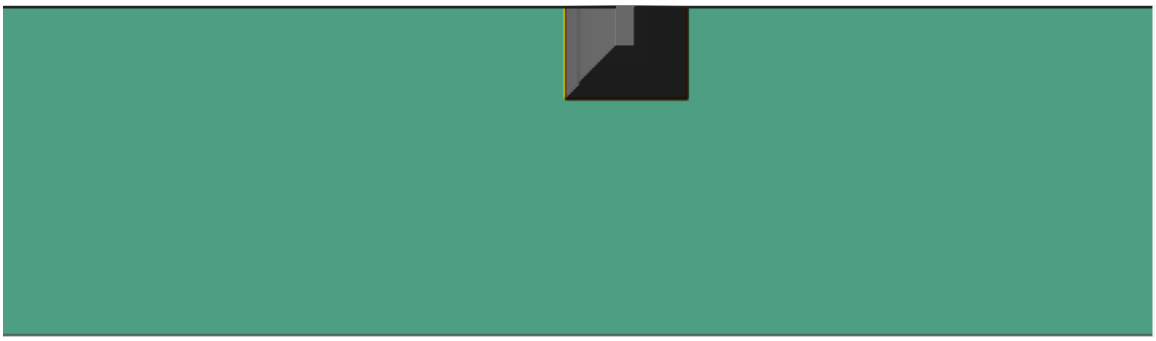

HEC-RAS Analysis Output (Flow Direction is left to right in all figures)

Run ID: S90-1b

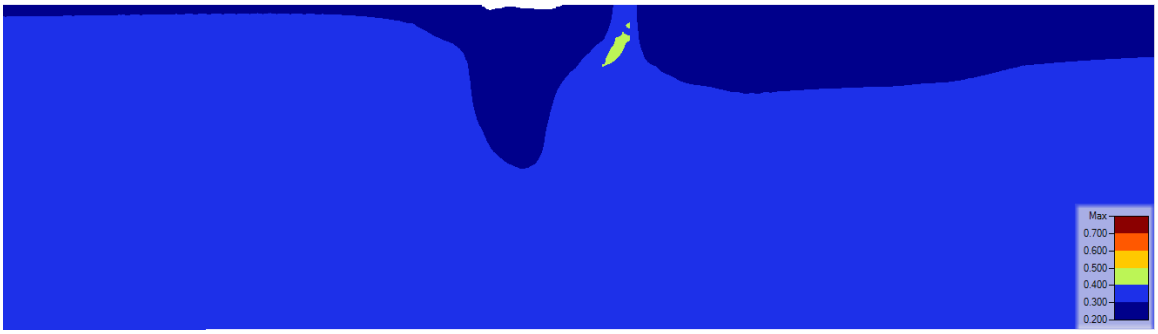

Run ID: S90-2b

Run ID: S90-3

Run ID: S90-4

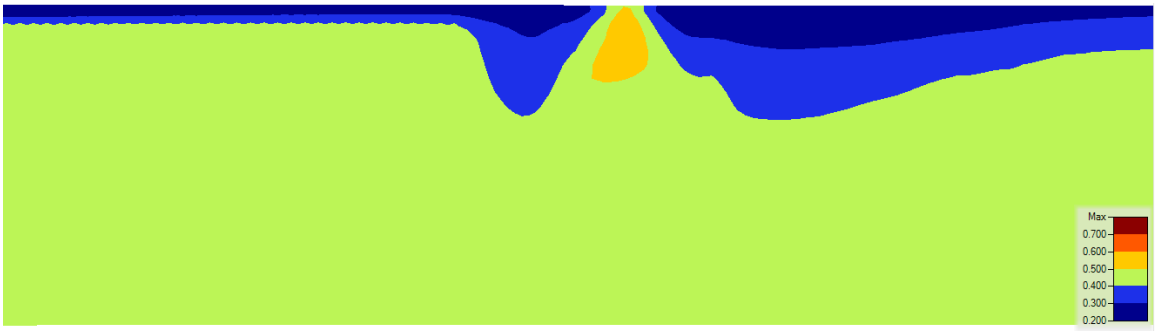

Run ID: L90-1

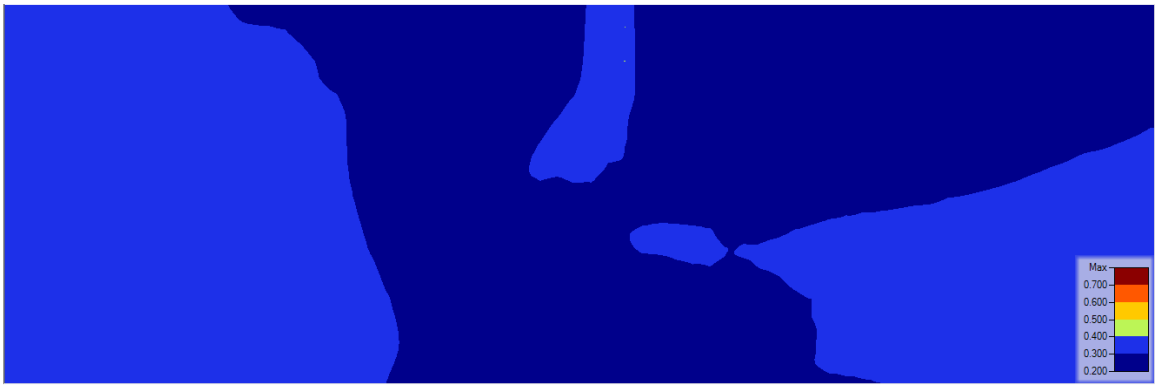

Run ID: L90-2

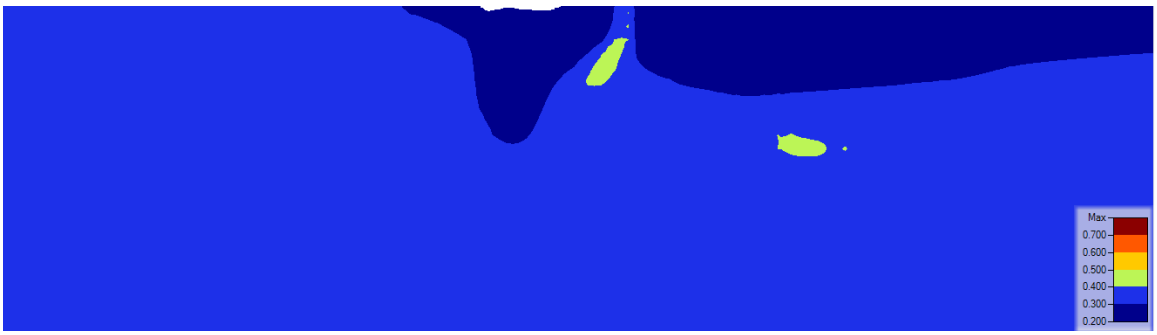

Run ID: L90-3

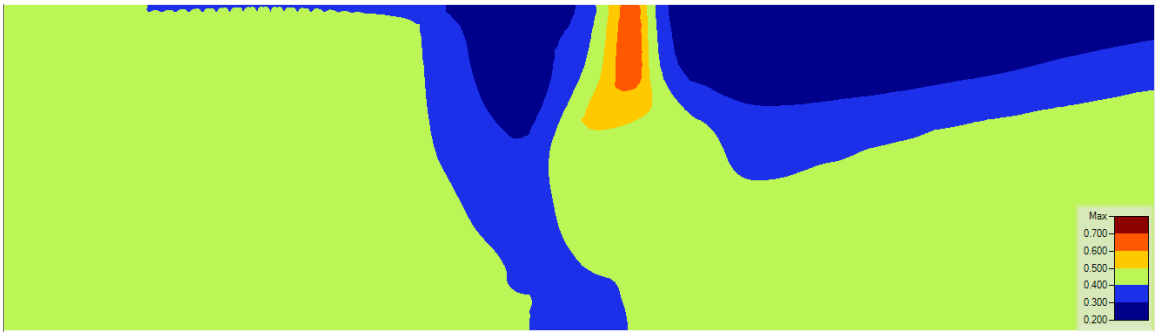

Run ID: L90-4

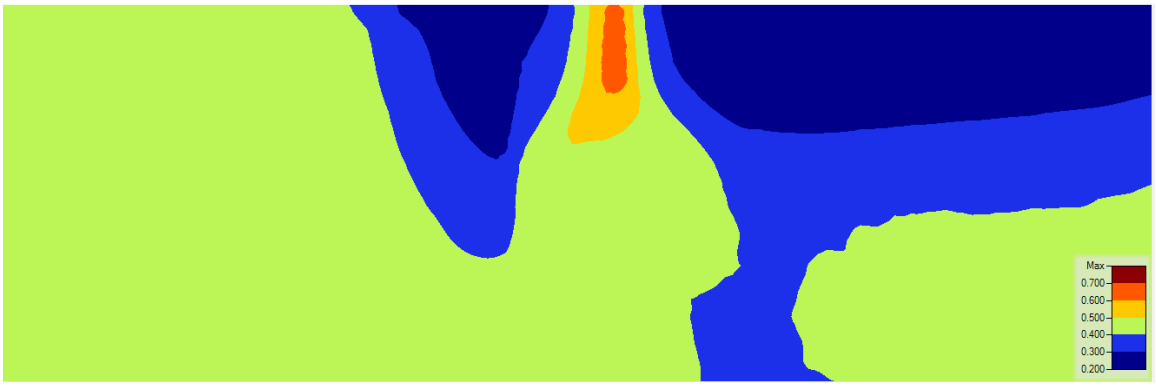

Appendix C

Equations

Conservation of Momentum – Newton's Second Law

$$\sum F_x = \frac{d\vec{M}}{dt}$$

Conservation of Momentum – Full Momentum

$$\frac{\partial v}{\partial t} + u\frac{\partial v}{\partial x} + v\frac{\partial v}{\partial y} = -g\frac{\partial H}{\partial y} + v_t\left(\frac{\partial^2 v}{dx^2} + \frac{\partial^2 v}{\partial y^2}\right) - c_f v + fu$$

$$\frac{\partial u}{\partial t} + u\frac{\partial u}{\partial x} + v\frac{\partial u}{\partial y} = -g\frac{\partial H}{\partial x} + v_t\left(\frac{\partial^2 u}{dx^2} + \frac{\partial^2 u}{\partial y^2}\right) - c_f u + fv$$

u, v: velocities in Cartesian directions

g: gravitational acceleration

v_t: horizontal eddy viscosity coefficient

c_f: bottom friction coefficient

f: Coriolis parameter

Conservation of Momentum – Diffusion Wave (A)

$$\frac{n^2|V|V}{\left(R(H)\right)^{4/3}} = -\nabla H$$

V: velocity vector

∇H: surface elevation gradient

n: Manning's n

Conservation of Momentum – Diffusion Wave (B)

$$\frac{\partial H}{\partial t} - \nabla \cdot \beta \nabla H + q = 0$$

Where: $\beta = \frac{(R(H))^{5/3}}{n|\nabla H|^{1/2}}$

Melville Original and Modified Scour Depth Equations (Melville, 1992)

(a) $$\frac{d_s}{Y_\infty} = 2K_M \eta^{(1-\delta)}$$

(b) $$\frac{d_s}{Y_\infty} = 1.12K_M \eta^{(1-\delta)}$$

Where:
$\eta = L/Y_\infty$
$\delta = 0$, if $\eta \leq 1$
$\delta = 0.5$, if $1 < \eta < 25$
$\delta = 1$, if $\eta \geq 25$
d_s = Maximum Scour Depth
Y_∞ = Depth of Approaching Flow
L = Length of Spur Dike
K_M = Shear Velocity Ratio

Scour Hole Volume (Kuhnle et al, 1999)

$$\frac{V_{30}}{(d_{s30})^3} = 17.106\left(\frac{L}{Y_\infty}\right)^{-0.781}$$

Where:
V_{30} = Scour Volume at 30 hr. (m^3)
d_{s30} = Maximum Depth of Scour (m)
L = Length of Spur Dike (m)
Y_∞ = Depth of Approaching Flow (m)

Scour Hole Dimensions from experimental runs (Kuhnle et al 1999)

Run Number	a/L	b/L	c/L	d/L	V_{30}/V_{sp}	Flow Rate
L90-1	4.0	0.8	1.9	6.0	11.0	Low
L90-2	4.0	0.7	1.7	4.9	7.7	Low
L90-3	3.4	0.0	1.6	7.7	11.2	High
L90-4	4.0	0.0	1.6	10.2	14.3	High
S90-1b	5.4	0.5	2.5	7.6	9.1	Low
S90-2b	4.0	1.0	1.0	4.7	2.4	Low
S90-3	4.5	0.7	1.6	5.8	4.8	High
S90-4	5.4	0.0	2.2	9.4	10.0	High

Scour Hole schematic (Kuhnle et al, 1999)